processes

MDPI

Article

Coordinated Dispatch Between Agricultural Park and Distribution Network: A Stackelberg Game Based on Carbon Emission Flow

Jiahao Gou, Hailong Cui and Xia Zhao *

State Key Laboratory of Power Transmission Equipment Technology, Chongqing University, Chongqing 400044, China; 20183080101125@cau.edu.cn (J.G.); chl@stu.cqu.edu.cn (H.C.)
* Correspondence: zx@cqu.edu.cn; Tel.: +86-138-9618-0133

Abstract

With the acceleration of global climate warming and agricultural modernization, the energy and carbon emission issues of agricultural parks (APs) have drawn increasing attention. An AP equipped with biogas-based combined heat and power (CHP) generation and photovoltaic systems serves as a prosumer terminal in a distribution network (DN). This paper introduces carbon emission flow (CEF) theory into the coordinated dispatch of APs and DNs. First, a CEF model for APs is established. Then, based on this model, a carbon–energy coordinated dispatch is carried out under bidirectional CEF interaction between the park and DN. A bidirectional carbon tax mechanism is adopted to explore the low-carbon synergy potential between them. Finally, the Stackelberg game approach is employed to address the pricing of electricity purchase/sale and carbon taxes in a DN, and the particle swarm optimization algorithm is used for rapid generating solutions. The case study shows that the proposed CEF model can effectively determine CEF distribution in the park. Moreover, the proposed bidirectional carbon tax mechanism significantly enhances the low-carbon economic benefits of both the AP and the DN.

Keywords: agricultural park; carbon emission flow; coordinated dispatch; carbon tax

check for updates

Academic Editor: Michael C. Georgiadis

Received: 26 May 2025
Revised: 13 June 2025
Accepted: 30 June 2025
Published: 2 July 2025

Citation: Gou, J.; Cui, H.; Zhao, X. Coordinated Dispatch Between Agricultural Park and Distribution Network: A Stackelberg Game Based on Carbon Emission Flow. *Processes* **2025**, *13*, 2102. https://doi.org/10.3390/pr13072102

Copyright: © 2025 by the authors. Licensee MDPI, Basel, Switzerland. This article is an open access article distributed under the terms and conditions of the Creative Commons Attribution (CC BY) license (https://creativecommons.org/licenses/by/4.0/).

1. Introduction

As global warming becomes severe, China has set a 'Carbon peaking and carbon neutrality' goal and incorporated it into the overall layout of ecological civilization construction and is building a new type of electric power system with new energy as the main body [1]. The low-carbon issue of power energy systems has reached an unprecedented level of importance. Globally, agricultural production accounts for 10–20% of total carbon emissions. Greenhouse (GH) costs make up 15–40% of total production costs [2]. The low-carbon energy management of APs has received widespread attention [3,4]. This paper investigates crop-cultivation APs incorporating GHs and other agricultural production loads, which operate as prosumer-enabling bidirectional power interactions with a DN. The GH needs the supply of CO_2, and the ventilation will dissipate CO_2 to cause carbon emission. Moreover, CHP can also cause carbon emission. Therefore, the coordinated dispatch of AP and DN is a low-carbon economic scheduling problem that requires a low-carbon target and carbon–energy coordination.

In the field of low-carbon scheduling of an AP with a DN, ref. [5] established an energy optimization model for GHs considering photovoltaic and CHP energy systems, aiming to

minimize operational costs. Ref. [3] defined the administrative boundaries of the park as the system boundary, accounting for direct carbon emission within boundaries, indirect emission originating from activities but occurring externally, as well as carbon reduction and sequestration activities. Ref. [6] developed a CO_2 flow model for GH micro-energy grids. It accounted for carbon emissions from energy use, CO_2 absorption, and emission from ventilation within GHs, establishing a low-carbon economic scheduling model. Ref. [7] established a GH model incorporating photovoltaic power generation, electric–thermal and biogas storage, and electric–thermal potential energy loads, utilizing blockchain technology to manage the operation of multi-GH parks and interaction with DNs.

With the application of game theory in multi-entity coordination in DNs [8], more studies are using game-theoretic approaches to study the interactions between APs and DNs. Ref. [9] proposed a method for optimizing multiple rural microgrids and DNs based on cooperative game theory. Ref. [10] studied the interaction and coordinated optimization between DN and agricultural irrigation parks using a Stackelberg game. Ref. [11] carried out photovoltaic low-carbon consumption under the coordination of a DN and AP in a Stackelberg game mode. However, most of these studies on low-carbon coordination between AP and DN have focused on the 'energy perspective' or 'low-carbon perspective'. There has been limited research from a 'carbon–energy perspective' on their coordinated operation.

To achieve low-carbon operation of power energy systems, analyzing and calculating carbon emissions is essential. Traditional methods using macro-statistical methods based on average emission factors are disconnected from the system's operating state, such as power flow distribution, and fail to effectively guide low-carbon operation. In contrast, carbon emission flow (CEF) theory [12] links low-carbon elements in power systems through CEF, offering new methods and tools for emission analysis.

As distributed generation integrates extensively into DNs, CEF and low-carbon scheduling of DNs are influenced by the demand side [13,14]. Ref. [15] studied low-carbon optimal operation methods for distribution systems based on CEF. Ref. [16] conducted low-carbon economic scheduling for medium- and low-voltage distribution systems using CEF theory. Ref. [17] presented a multi-microgrid system method for tracing CEFs in DNs and coupled it with carbon–energy trading. At the park level, most existing CEF models focus on energy production/conversion and storage [18,19]. However, significant gaps remain in models with CHP, including carbon capture [20]. Additionally, while many studies explore electricity–carbon trading between prosumers in DNs [17,21], how to calculate the carbon intensity of prosumers' reverse electricity exported to DNs has not been detailed [22–25].

In most studies, the carbon intensity at the connection node between parks and DN is treated as the boundary condition for scheduling models. This approach only considers carbon emission flowing from the DN to the park, ignoring the park's impact on the network's carbon emission distribution. In reality, most industrial and commercial parks are prosumers that interact with carbon emission bidirectionally with the DN. Although Ref. [17] considered bidirectional CEF in a microgrid-DN scheduling model, it treated the microgrid as just a power source. The interaction was still limited to electricity and price, without leveraging CEF information to promote low-carbon coordination.

Since the CEF theory was introduced, its application in AP and coordination with DN remains underreported. This paper applies CEF theory to carbon–energy-coordinated scheduling of AP and DN. The key contributions are as follows:

(1) The CEF modeling for APs is refined, which improves the CEF of CHP. Also, a method is proposed to calculate the carbon intensity of electricity exported to DNs from APs considered emissions from GHs.

(2) A bidirectional carbon tax-based integrated energy–carbon pricing mechanism is proposed which considers interactive carbon flows between DNs and APs. A Stackelberg game framework dynamically optimizes electricity prices and carbon taxes, with particle swarm optimization employed for equilibrium solutions.

(3) The proposed model is validated using IEEE 33-node distribution and an AP connected at node 24. The results show that the CEF model of APs considering GH carbon emissions can solve the carbon intensity of electricity exported to DNs. Based on the results, the effectiveness of the bidirectional carbon tax mechanism proposed in this paper in the carbon–energy coordinated scheduling of the DN and the park is verified.

This paper is organized as follows: Section 2 details the CEF model of the AP. Section 3 presents the low-carbon Stackelberg game scheduling model and its solution approach for the AP and DN. Case studies are provided in Section 4. Finally, Section 5 summarizes the findings. The hierarchical block diagrams of the models in each section of this paper are presented in Figure 1.

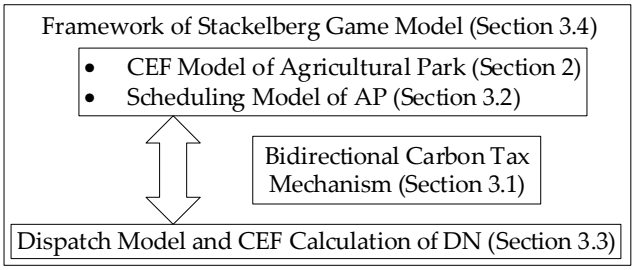


Figure 1. Hierarchical module diagram of the article.

2. Energy Flow and CEF Model of Agricultural Park

2.1. Energy Flow Model of Agricultural Park

As illustrated in Figure 2, the energy facilities in this study for AP consist of a biogas CHP system equipped with a carbon capture device (CC-CHP), an electric boiler, and an electricity/heat/CO_2 storage system. On the park user side, there are GH and other agricultural production loads with demands for electricity, heat, and CO_2 (GH).

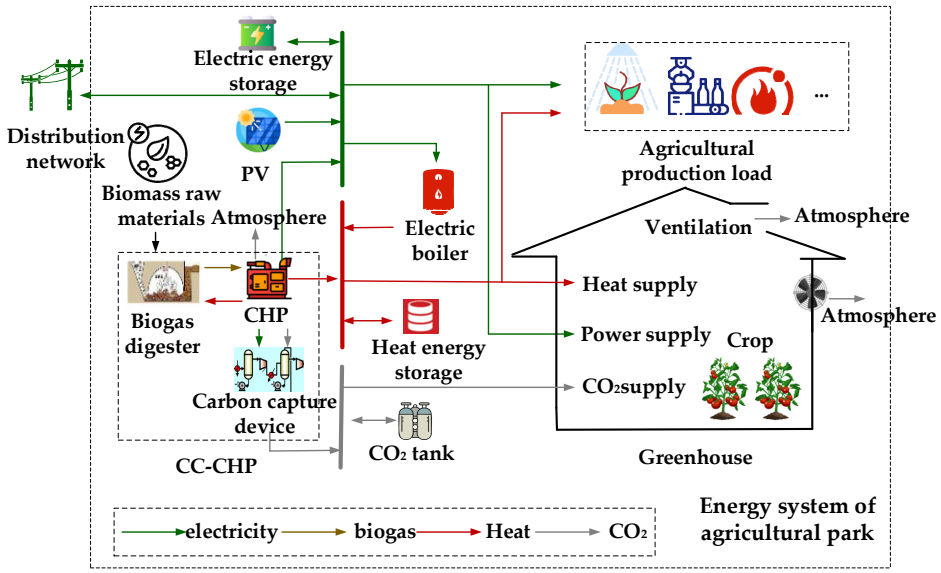


Figure 2. Schematic diagram of the agricultural park (AP).

2.1.1. Model of CC-CHP

Within the park, a biogas fermentation pond is installed to heat the purchased biomass raw materials, triggering a reaction that generates biogas. The gas yield is temperature-controlled. The rate of biogas production can be regulated by managing the temperature of the biogas pond and the feedstock input [26]:

$$\begin{cases} q_{\mathrm{bio},t} = f_{\mathrm{bio},t} q_{\mathrm{slu},t} \Delta t / 24 \\ f_{\mathrm{bio},t} = a(T_{\mathrm{tem},t} - T_{\mathrm{o}})^2 + b \\ T_{\mathrm{tem}}^{\min} \le T_{\mathrm{tem},t} \le T_{\mathrm{tem}}^{\max} \end{cases} \tag{1}$$

where $q_{\mathrm{bio},t}$ and $q_{\mathrm{slu},t}$ are the biogas and slurry flow rates, respectively; $f_{\mathrm{bio},t}$ denotes the daily biogas production rate, which is a quadratic function of temperature; $T_{\mathrm{tem},t}$ is the fermentation temperature; T_{o} is the optimal fermentation temperature (set to 37 °C in this study), and a and b are the coefficients obtained from the data fitting [27].

Maintaining the temperature in the biogas reactor requires continuous heating to compensate for both the heat loss from the reactor and the heat demand for material input:

$$\begin{cases} m_{\mathrm{bms},t} / \Delta t = n_{\mathrm{OLR}} q_{\mathrm{slu},t} \Delta t / 24 \beta_1 \beta_2 \\ P_{\mathrm{slu},t}^{\mathrm{h}} = c_{\mathrm{slu}} M_{\mathrm{bms},t} (T_{\mathrm{tem},t} - T_{\mathrm{out}}) / \Delta t \\ P_{\mathrm{med},t}^{\mathrm{h}} = k_{\mathrm{a}} A_{\mathrm{s}} (T_{\mathrm{tem},t} - T_{\mathrm{out}}) \\ P_{\mathrm{cog},t}^{\mathrm{h}} = P_{\mathrm{slu},t}^{\mathrm{h}} + P_{\mathrm{med},t}^{\mathrm{h}} \end{cases} \tag{2}$$

where $m_{\mathrm{bms},t}$ is the mass of the raw biomass material; n_{OLR} denotes the organic loading rate in the slurry; β_1 and β_2 are the content of raw material in the biomass slurry and the content of organic matter in the raw material, respectively. $P_{\mathrm{slu},t}^{\mathrm{h}}$ and $P_{\mathrm{med},t}^{\mathrm{h}}$ are the heat required for material heating and loss; c_{slu} and T_{out} are the specific heat capacity of the slurry and the ambient temperature; k_{a} and A_{s} are the heat dissipation coefficient and area of the biogas reactor; $P_{\mathrm{cog},t}^{\mathrm{h}}$ is the total heat required by the biogas reactor.

The CHP model utilizing biogas as fuel is as follows:

$$\begin{cases} P_{\mathrm{bio},t} = q_{\mathrm{bio},t} L_{\mathrm{bio}} \\ P_{\mathrm{CHP},t}^{\mathrm{e0}} = P_{\mathrm{bio},t} \eta_{\mathrm{CHP}}^{\mathrm{e}} \\ P_{\mathrm{CHP},t}^{\mathrm{h0}} = P_{\mathrm{bio},t} \eta_{\mathrm{CHP}}^{\mathrm{h}} \end{cases} \tag{3}$$

where $P_{\mathrm{bio},t}$ is the total power output after the combustion of biogas; L_{bio} denotes the lower heating value of the biogas; $P_{\mathrm{CHP},t}^{\mathrm{e0}}$ and $P_{\mathrm{CHP},t}^{\mathrm{h0}}$ are the total electrical and heat outputs from CHP; $\eta_{\mathrm{CHP}}^{\mathrm{e}}$ and $\eta_{\mathrm{CHP}}^{\mathrm{h}}$ are the electrical and heat efficiencies of CHP.

Moreover, the biogas fermentation pond is constrained by the gas production rate, and the simultaneous generation of electricity and heat is limited by ramping capabilities:

$$\begin{cases} U_{\mathrm{bio},t} q_{\mathrm{bio}}^{\min} \le q_{\mathrm{bio},t} \le U_{\mathrm{bio},t} q_{\mathrm{bio}}^{\max} \\ P_{\mathrm{CHP},t}^{\mathrm{h}} = P_{\mathrm{CHP},t}^{\mathrm{h0}} - P_{\mathrm{slu},t}^{\mathrm{h}} - P_{\mathrm{med},t}^{\mathrm{h}} \ge 0 \\ -D_{\mathrm{CHP}}^{\mathrm{e,down}} \Delta t \le P_{\mathrm{CHP},t}^{\mathrm{e0}} - P_{\mathrm{CHP},t-1}^{\mathrm{e0}} \le D_{\mathrm{CHP}}^{\mathrm{e,up}} \Delta t \\ -D_{\mathrm{CHP}}^{\mathrm{h,down}} \Delta t \le P_{\mathrm{CHP},t}^{\mathrm{h0}} - P_{\mathrm{CHP},t-1}^{\mathrm{h0}} \le D_{\mathrm{CHP}}^{\mathrm{h,up}} \Delta t \end{cases} \tag{4}$$

where $U_{\mathrm{bio},t}$ is the biogas intake state variable; $P_{\mathrm{CHP},t}^{\mathrm{h}}$ denotes the net excess heat output from CHP; $D_{\mathrm{CHP}}^{\mathrm{e,up}}$, $D_{\mathrm{CHP}}^{\mathrm{e,down}}$, $D_{\mathrm{CHP}}^{\mathrm{h,up}}$, and $D_{\mathrm{CHP}}^{\mathrm{h,down}}$ are the upper and lower ramping constraints for electricity and heat production, respectively.

The carbon capture device is for the sequestration of CO_2 produced by CHP, with the power consumption and capture rate relationship detailed as follows [28]:

$$\begin{cases} P_{\mathrm{cap},t} = U_{\mathrm{cap},t}(P^{\mathrm{a}}_{\mathrm{cap}} + P^{\mathrm{op}}_{\mathrm{cap},t}) \\ P^{\mathrm{op}}_{\mathrm{cap},t} = \lambda_{\mathrm{e}} R_{\mathrm{cap},t} \\ R_{\mathrm{cap},t} = \eta_{\mathrm{cap},t}\rho_{\mathrm{bio}} P_{\mathrm{bio},t} \end{cases} \tag{5}$$

where $P_{\mathrm{cap},t}$ is the power of the carbon capture device; $P^{\mathrm{a}}_{\mathrm{cap}}$ and $P^{\mathrm{op}}_{\mathrm{cap},t}$ denote the fixed and variable power, respectively; $U_{\mathrm{cap},t}$ is the operational status variable. The variable energy consumption is the product of the electricity consumed per unit mass of CO_2 captured (λ_{e}) and the CO_2 capture rate ($R_{\mathrm{cap},t}$). The CO_2 capture rate is the product of the carbon capture efficiency ($\eta_{\mathrm{cap},t}$), the input power of biogas, and its carbon intensity (ρ_{bio}).

The carbon capture unit is powered by the CHP, and its capture rate is bounded by the following:

$$\begin{cases} P^{\mathrm{e}}_{\mathrm{CHP},t} = P^{\mathrm{e0}}_{\mathrm{CHP},t} - P_{\mathrm{cap},t} \geq 0 \\ \eta^{\min}_{\mathrm{cap}} U_{\mathrm{cap},t} \leq \eta_{\mathrm{cap},t} \leq \eta^{\max}_{\mathrm{cap}} U_{\mathrm{cap},t} \end{cases} \tag{6}$$

where $P^{\mathrm{e}}_{\mathrm{CHP},t}$ is the net excess electrical energy output from CHP, while $\eta^{\max}_{\mathrm{cap}}$ and $\eta^{\min}_{\mathrm{cap}}$ denote the minimum and maximum limits of the carbon capture rate.

2.1.2. Electric Boiler and Electricity/Heat/CO_2 Storage

The electric boiler is an energy conversion device, which transforms electricity into heat energy. The corresponding model is presented as follows:

$$\begin{cases} P^{\mathrm{h}}_{\mathrm{eb},t} = U_{\mathrm{eb},t} P^{\mathrm{e}}_{\mathrm{eb},t} \eta_{\mathrm{eb}} \\ P^{\mathrm{h,min}}_{\mathrm{eb},t} \leq P^{\mathrm{h}}_{\mathrm{eb},t} \leq P^{\mathrm{h,max}}_{\mathrm{eb},t} \\ -D^{\mathrm{down}}_{\mathrm{eb}} \Delta t \leq P^{\mathrm{h}}_{\mathrm{eb},t} - P^{\mathrm{h}}_{\mathrm{eb},t-1} \leq D^{\mathrm{up}}_{\mathrm{eb}} \Delta t \end{cases} \tag{7}$$

where $U_{\mathrm{eb,t}}$ denotes the operational status of the electric boiler; $P^{\mathrm{e}}_{\mathrm{eb},t}$ is the power consumption of the electric boiler; η_{eb} is the electricity-to-heat conversion efficiency; $P^{\mathrm{h}}_{\mathrm{eb},t}$ is the heat output. The output power and operation of the device must satisfy the upper and lower limits of the equipment's power output and operational constraints; $P^{\mathrm{h,max}}_{\mathrm{eb},t}$ and $P^{\mathrm{h},min}_{\mathrm{eb},t}$ are the upper and lower limits of the electric boiler's heat output; $D^{\mathrm{up}}_{\mathrm{eb}}$ and $D^{\mathrm{down}}_{\mathrm{eb}}$ are the upper limits of the boiler's ramp-up and ramp-down rates, respectively.

The model of the energy storage (ES) devices for electricity/heat/CO_2 is as follows, which is determined by the energy stored in the previous period $E_{\mathrm{bt},t-1}$ and the product of the power change in this period and time:

$$\begin{cases} E_{\mathrm{bt},t} = (1-\sigma_{\mathrm{bt}})E_{\mathrm{bt},t-1} + \left(P^{\mathrm{cha}}_{\mathrm{bt},t}\eta^{\mathrm{cha}}_{\mathrm{bt}} - P^{\mathrm{dis}}_{\mathrm{bt},t}/\eta^{\mathrm{dis}}_{\mathrm{bt}}\right)\Delta t \\ E_{\mathrm{hr},t} = (1-\sigma_{\mathrm{hr}})E_{\mathrm{hr},t-1} + \left(P^{\mathrm{cha}}_{\mathrm{hr},t}\eta^{\mathrm{cha}}_{\mathrm{hr}} - P^{\mathrm{dis}}_{\mathrm{hr},t}/\eta^{\mathrm{dis}}_{\mathrm{hr}}\right)\Delta t \\ N_{\mathrm{ct},t} = N_{\mathrm{ct},t-1} + \left(R^{\mathrm{cha}}_{\mathrm{ct},t} - R^{\mathrm{dis}}_{\mathrm{ct},t}\right)\Delta t \end{cases} \tag{8}$$

where $E_{\mathrm{bt},t}$, $E_{\mathrm{hr},t}$, and $N_{\mathrm{ct},t}$ are the stored electricity/heat energy and the amount of CO_2 in carbon storage, respectively; σ_{bt} and σ_{hr} denote the self-discharge/heat loss rates of the electricity/heat storage; $P^{\mathrm{cha}}_{\mathrm{bt},t}$, $P^{\mathrm{dis}}_{\mathrm{bt},t}$, $P^{\mathrm{cha}}_{\mathrm{hr},t}$, $P^{\mathrm{dis}}_{\mathrm{hr},t}$, $R^{\mathrm{cha}}_{\mathrm{ct},t}$, and $R^{\mathrm{dis}}_{\mathrm{ct},t}$ are the charging/discharging power of electricity/heat and the charging/discharging rate of CO_2, respectively; $\eta^{\mathrm{cha}}_{\mathrm{bt}}$, $\eta^{\mathrm{dis}}_{\mathrm{bt}}$, $\eta^{\mathrm{cha}}_{\mathrm{hr}}$ and $\eta^{\mathrm{cha}}_{\mathrm{hr}}$ are the charging/discharging efficiency of electricity/heat storage.

Each ES component is subject to operational constraints. Taking electrical ES as an example, these include upper and lower limits on charging/discharging rates, mutual

exclusivity of charging and discharging, storage capacity limits, and conservation of stored energy over the dispatch period.

$$\begin{cases} U_{\mathrm{bt},t}^{\mathrm{cha}} P_{\mathrm{bt}}^{\mathrm{cha,min}} \le P_{\mathrm{bt},t}^{\mathrm{cha}} \le U_{\mathrm{bt},t}^{\mathrm{cha}} P_{\mathrm{bt}}^{\mathrm{cha,max}} \\ U_{\mathrm{bt},t}^{\mathrm{dis}} P_{\mathrm{bt}}^{\mathrm{dis,min}} \le P_{\mathrm{bt},t}^{\mathrm{dis}} \le U_{\mathrm{bt},t}^{\mathrm{dis}} P_{\mathrm{bt}}^{\mathrm{dis,max}} \\ U_{\mathrm{bt},t}^{\mathrm{cha}} + U_{\mathrm{bt},t}^{\mathrm{dis}} \le 1 \\ E_{\mathrm{bt}}^{\min} \le E_{\mathrm{bt},t} \le E_{\mathrm{bt}}^{\max} \\ E_{\mathrm{bt},0} = E_{\mathrm{bt},24} \end{cases} \tag{9}$$

where $P_{\mathrm{bt}}^{\mathrm{dis,max}}$ and $P_{\mathrm{bt}}^{\mathrm{dis,min}}$ are the upper limits of charging and discharging power, respectively; $U_{\mathrm{bt},t}^{\mathrm{cha}}$ and $U_{\mathrm{bt},t}^{\mathrm{dis}}$ are the charging and discharging status variables; $E_{\mathrm{bt}}^{\max}$ and $E_{\mathrm{bt}}^{\min}$ are the upper and lower limits of the storage capacity; $E_{\mathrm{bt},0}$ is the initial storage capacity; $E_{\mathrm{bt},24}$ is the storage capacity at the end of one day of charging and discharging.

2.1.3. Balance of Electricity/Heat/CO_2 in AP

Within the park, it is necessary to meet the CO_2 supply for GHs and the energy supply for loads, thus ensuring the balance between energy and CO_2 supply is maintained.

$$\begin{cases} P_{\mathrm{grid},t} + P_{\mathrm{pv},t} + P_{\mathrm{CHP},t}^{\mathrm{e0}} - P_{\mathrm{cap},t} + P_{\mathrm{bt},t}^{\mathrm{dis}} = P_{\mathrm{cut},t} + P_{\mathrm{eb},t}^{\mathrm{e}} + P_{\mathrm{bt},t}^{\mathrm{cha}} + P_{\mathrm{GH},t}^{\mathrm{e}} + P_{\mathrm{L},t}^{\mathrm{e}} \\ P_{\mathrm{CHP},t}^{\mathrm{h0}} - P_{\mathrm{slu},t}^{\mathrm{h}} - P_{\mathrm{bms},t}^{\mathrm{h}} + P_{\mathrm{eb},t}^{\mathrm{h}} + P_{\mathrm{hr},t}^{\mathrm{dis}} = P_{\mathrm{hr},t}^{\mathrm{cha}} + P_{\mathrm{GH},t}^{\mathrm{h}} + P_{\mathrm{L},t}^{\mathrm{h}} \\ R_{\mathrm{cap},t}\Delta t + R_{\mathrm{ct},t}^{\mathrm{dis}}\Delta t = R_{\mathrm{ct},t}^{\mathrm{cha}}\Delta t + R_{\mathrm{inj},t}\Delta t \end{cases} \tag{10}$$

where $P_{\mathrm{grid},t}$ is the power interaction between the AP and the DN (positive for power input to the park). Due to the inability of the park's power dispatching to fully absorb the photovoltaic power within the park, there is a solar power curtailment. $P_{\mathrm{pv},t}$ and $P_{\mathrm{cut},t}$ denote the photovoltaic output and curtailed power; $P_{\mathrm{GH},t}^{\mathrm{e}}$ and $P_{\mathrm{GH},t}^{\mathrm{h}}$ are the electrical and heat loads of the GH; $R_{\mathrm{inj},t}$ is the CO_2 requirement of the GH; $P_{\mathrm{L},t}^{\mathrm{e}}$ and $P_{\mathrm{L},t}^{\mathrm{h}}$ are the electrical/heat demands of the production load.

The power interaction with the DN must be within the maximum power limit $P_{\mathrm{grid},t}^{\max}$ and the curtailed photovoltaic power $P_{\mathrm{cut},t}$ must be greater than zero:

$$\begin{cases} -P_{\mathrm{grid},t}^{\max} \le P_{\mathrm{grid},t} \le P_{\mathrm{grid},t}^{\max} \\ P_{\mathrm{cut},t} \ge 0 \end{cases} \tag{11}$$

To distinguish between the scenarios of the park purchasing electricity from the DN and selling surplus electricity back to the grid, the following constraints are introduced:

$$\begin{cases} P_{\mathrm{d2p},t} - P_{\mathrm{p2d},t} = P_{\mathrm{grid},t} \\ 0 \le P_{\mathrm{d2p},t} \le M(1 - U_{\mathrm{p2d},t}) \\ 0 \le P_{\mathrm{p2d},t} \le MU_{\mathrm{p2d},t} \end{cases} \tag{12}$$

where $P_{\mathrm{d2p},t}$ and $P_{\mathrm{p2d},t}$ are the electricity purchase and sale from the DN to the park, respectively; $U_{\mathrm{p2d},t}$ is a binary (0 or 1) indicator variable representing the park's electricity purchase/sale status (0 for purchase, 1 for sale); M is a sufficiently large positive real number.

2.2. CEF Model of Agricultural Park

The distribution of CEF follows the energy flow within the AP, as shown in Figure 3.

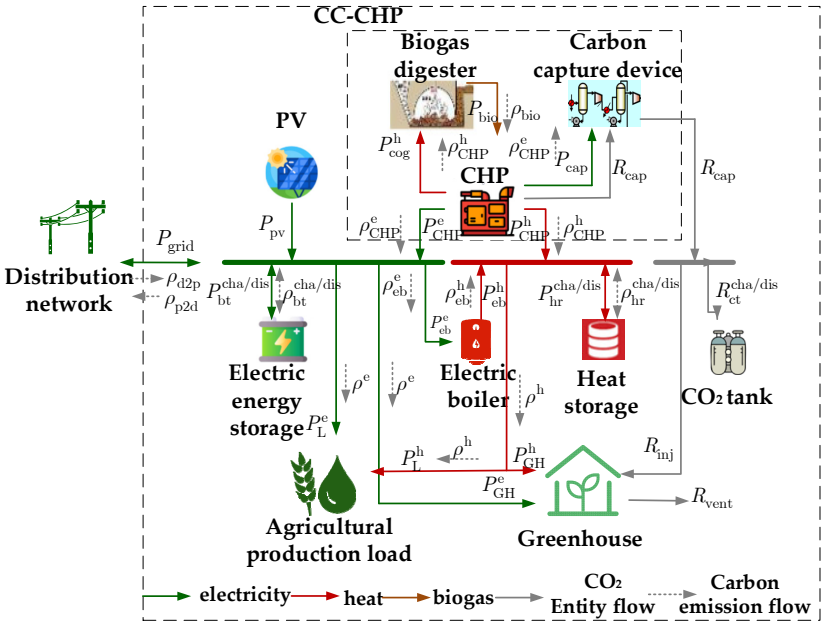


Figure 3. Distribution of CEF in AP.

In Figure 3, solid lines denote the flows of electrical and heat energy, as well as CO_2, while dashed gray lines represent CEF. To facilitate the subsequent description of the flows, Figure 3 also labels the rates of electrical and heat output (e.g., P^{e}_{CHP} and P^{h}_{CHP} denote the electrical and heat output by the CHP, respectively), CO_2 entity flow rates (e.g., R_{cap} indicates the CO_2 flow rate from the carbon capture device, with units of $kgCO_2/h$), and CEF intensity (e.g., ρ^{e}_{CHP} and ρ^{h}_{CHP} are the carbon intensity associated with the CHP's electrical and heat output, respectively, with units of $kgCO_2/kWh$).

Virtual carbon emission does not incur loss under energy flow. From the perspective of energy equipment, the total carbon emissions at the input and output ports are consistent. Based on the principle of carbon conservation of the CEF energy flow and conversion relationships, a CEF model for various energy devices within the park can be established.

2.2.1. CEF Model of CC-CHP

Existing research (e.g., ref. [20]) has proposed a CEF model for CC-CHP as follows:

$$\begin{cases} \rho_{bio} P_{bio,t} - R_{cap,t} = \rho^{e0}_{CHP,t} P^{e0}_{CHP,t} + \rho^{h}_{CHP,t} P^{h}_{CHP,t} \\ \rho^{e}_{CHP,t} P^{e}_{CHP,t} \Delta t = \rho^{e0}_{CHP,t} P^{e0}_{CHP,t} \Delta t \\ P^{e}_{CHP,t} = P^{e0}_{CHP,t} - P_{cap,t} \end{cases} \tag{13}$$

where $P^{e0}_{CHP,t}$ is the total electrical power output of CHP; $\rho^{e0}_{CHP,t}$ and $\rho^{h}_{CHP,t}$ denote the carbon densities of the total electrical and thermal outputs; $P^{e}_{CHP,t}$ and $\rho^{e}_{CHP,t}$ are the net excess electrical power output and the carbon intensity of the net excess electrical energy.

The model in ref. [20] does not account for the CEF associated with the power of a carbon capture device. This violates the consistency principle of CEF theory, which dictates that the carbon densities of branches exiting the same node should be uniform.

To address this, this paper considers the CEF related to the power of the carbon capture device and further considers the heat consumption of the biogas reactor. A CEF model for biogas with carbon capture is established, as depicted in Figure 4.

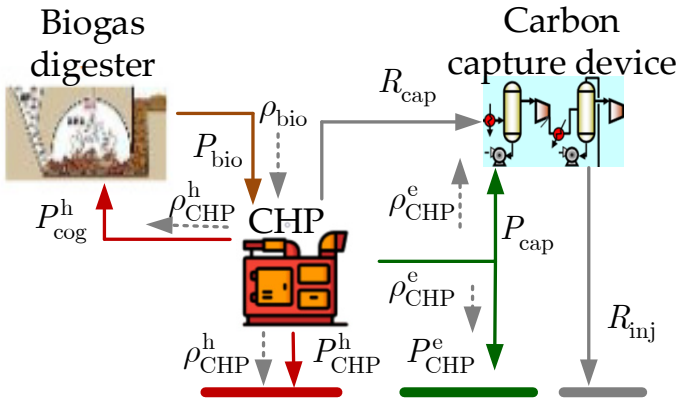


Figure 4. CEF model of CHP systems containing carbon capture.

In the CC-CHP system, carbon emissions at the input include biogas fuel, electricity consumption for carbon capture, and heat consumption of the biogas reactor. At the output, carbon emission comprises the total carbon emission from the system's electrical and thermal outputs, as well as the CO_2 captured. The model ensures the principle of consistent carbon intensity across branches exiting the CHP.

$$\rho_{bio}P_{bio,t} + \rho^{e}_{CHP,t}P_{cap,t} + \rho^{h}_{CHP,t}(P^{h}_{slu,t} + P^{h}_{med,t}) = \rho^{e}_{CHP,t}P^{e0}_{CHP,t} + \rho^{h}_{CHP,t}P^{h0}_{CHP,t} + R_{cap,t} \tag{14}$$

where ρ_{bio} denotes the carbon intensity of biogas; $\rho^{e}_{CHP,t}$ and $\rho^{h}_{CHP,t}$ are the carbon densities of the CHP's electrical and thermal energy outputs, respectively.

The inverse relationship between the carbon intensity at the output port and efficiency leads to uniform electrical/thermal carbon densities at the CHP output port:

$$\begin{cases} \rho^{e}_{CHP,t} = \dfrac{\rho_{bio}P_{bio,t} - R_{cap,t}}{2\eta^{e}_{CHP}P_{bio,t} - R_{cap,t} - P^{h}_{cog,t}\eta^{e}_{CHP}/\eta^{h}_{CHP}} \\ \rho^{h}_{CHP,t} = \dfrac{\rho_{bio}P_{bio,t} - R_{cap,t}}{2\eta^{h}_{CHP}P_{bio,t} - R_{cap,t}\eta^{h}_{CHP}/\eta^{e}_{CHP} - P^{h}_{cog,t}} \end{cases} \tag{15}$$

2.2.2. CEF Model for Other Energy Equipment in AP

1. PV

The electricity generated by photovoltaic (PV) systems within the park originates from solar radiation and is considered a clean energy source. This paper posits that its carbon emission intensity is zero.

2. Electric boiler

The electric boiler converts electrical energy into thermal energy, with the CEF also flowing from electrical to thermal energy:

$$\rho^{e}_{eb,t}P^{e}_{eb,t}\Delta t = \rho^{h}_{eb,t}P^{h}_{eb,t}\Delta t \tag{16}$$

where $\rho^{e}_{eb,t}$ and $\rho^{h}_{eb,t}$ are the carbon densities of electrical and thermal energy at the input and output ports of the electric boiler, respectively.

3. Electrical/Heat ES

The CEF model for ES must account for energy losses and efficiencies during charging and discharging, as formulated below [20]:

$$\begin{cases} R^{e,cha}_{t} = \rho^{e,cha}_{t}P^{cha}_{bt,t} \\ R^{e,dis}_{t} = \rho^{e}_{ess,t}P^{dis}_{bt,t} = \rho^{ce}_{ess,t-1}P^{dis}_{bt,t}/\eta^{dis}_{bt} \\ \rho^{ce}_{ess,t} = (\rho^{ce}_{ess,t-1}E_{bt,t-1} + R^{cha}_{bt,t} - R^{dis}_{bt,t})/E_{bt,t} \end{cases} \tag{17}$$

where $R_t^{e,cha}$ and $R_t^{e,dis}$ is the carbon emission charged and discharged during period t; $\rho_t^{e,cha}$ is the carbon intensity of charging; $\rho_{ess,t}^{e}$ is the carbon intensity of the ES when discharging to the external; $\rho_{ess,t}^{ce}$ is the storage's load carbon rate, indicating the actual carbon intensity discharged by the storage. The CEF model and meaning of each variable for thermal ES is analogous to that of electricity storage (the meanings of the variables are similar):

$$\begin{cases} R_t^{h,cha} = \rho_t^{h,cha} P_{hr,t}^{cha} \Delta t \\ R_t^{h,dis} = \rho_{ess,t}^{h} P_{hr,t}^{dis} \Delta t = \rho_{ess,t-1}^{ch} P_{hr,t}^{dis} / \eta_{hr}^{dis} \\ \rho_{ess,t}^{ch} = (\rho_{ess,t-1}^{ch} E_{hr,t-1} + R_{hr,t}^{cha} - R_{hr,t}^{dis}) / E_{hr,t} \end{cases} \tag{18}$$

2.2.3. Carbon Intensity Calculation of the Electrical/Heat Power Supplied to Park Users

Calculate CEF results based on the energy flow outcomes within the park. The carbon intensity of electrical energy is computed as follows: First, determine the carbon intensity of electricity produced by the CHP, as shown in Equation (15); Next, calculate the carbon intensity supplied by the CHP, PV, and DN, as per Equation (19), where $\rho_{d2p,t}$ is the carbon intensity (the carbon emission intensity of nodes) at the park's connection node to the DN. This intensity also serves as the carbon intensity during the charging period of electrical ES:

$$\rho_t^{e,cha} = \frac{\rho_{d2p,t} P_{grid,t} + \rho_{CHP,t}^{e} P_{CHP,t}^{e}}{P_{grid,t} + P_{pv,t} - P_{cut,t} + P_{CHP,t}^{e}} \tag{19}$$

Subsequently, calculate the discharge carbon intensity of the electrical ES. Utilizing Equations (17) and (19), the load carbon rate of the electrical ES can be derived, and further yields its output electrical energy carbon intensity:

$$\rho_{ess,t}^{e} = \rho_{ess,t-1}^{ce} / \eta_{dis}^{bt} \tag{20}$$

Finally, calculate the carbon intensity of electricity in the park. Equations (15), (19) and (20) allow for the determination of the carbon intensity of the park's electricity:

$$\rho_t^{e} = \frac{\rho_{d2p,t} P_{grid,t} + \rho_{CHP,t}^{e} P_{CHP,t}^{e} + \rho_{ess,t}^{e} P_{bt,t}^{dis}}{P_{grid,t} + P_{pv,t} - P_{cut,t} + P_{CHP,t}^{e} + P_{bt,t}^{dis}} \tag{21}$$

The calculation for heat energy carbon intensity is similar to that for electrical energy.

$$\begin{cases} \rho_{eb,t}^{h} = \frac{\rho_t^{e}}{\eta_{eb}},\ \rho_t^{h,cha} = \frac{\rho_{CHP,t}^{h} P_{CHP,t}^{h} + \rho_{eb,t}^{h} P_{eb,t}^{h}}{P_{CHP,t}^{h} + P_{eb,t}^{h}} \\ \rho_{ess,t}^{h} = \frac{\rho_{ess,t-1}^{ch}}{\eta_{hr}^{dis}},\ \rho_t^{h} = \frac{\rho_{CHP,t}^{h} P_{CHP,t}^{h} + \rho_{eb,t}^{h} P_{eb,t}^{h} + \rho_{ess,t}^{h} P_{hr,t}^{dis}}{P_{CHP,t}^{h} + P_{eb,t}^{h} + P_{hr,t}^{dis}} \end{cases} \tag{22}$$

2.3. Carbon Intensity Calculation of Power Exported from AP to DN

In accordance with the CEF theory, the carbon intensity of a node characterizes the carbon emission intensity at that node, which reflects the aggregate cleanliness of the power supplied to the node from various branches. The carbon intensity of branches exiting node *i* is equivalent to the carbon intensity of node *i.* When the park purchases electricity from the DN, the carbon intensity at the park's connection node is determined by the distribution of CEF within the network. This section tackles the issue of calculating the carbon intensity for the AP's surplus electricity exported to the DN.

The CO_2 emission of parks consists of two parts (as shown in Figure 3). The CO_2 not captured from CHP and CO_2 produced by crop respiration is released into the atmosphere via exhaust fans/ventilation windows. The uncaptured CO_2 from CHP is attached to the electrical and thermal power outputs of CHP in the form of CEF, whereas the carbon

emission from the GH is not reflected in the emission flows. According to the modeling philosophy of CEF, attaching the carbon emission from GH to the electricity sales power of the AP to the DN in the form of virtual CEF presents a solution. However, carbon emissions from GHs may occur during both the park's electricity purchase and sales periods. Based on the CEF model of ES devices (Equations (17) and (18)), this paper proposes an accumulation-and-allocation method for carbon emissions from GHs. It accumulates the carbon emissions from GHs during the park's electricity purchase period and subsequently allocates them to the adjacent electricity sales periods of the park. These emissions are then combined with the carbon emission from GH during the sales period and included in the CEF of the park's electricity sales power, as fundamentally illustrated in Figure 5.

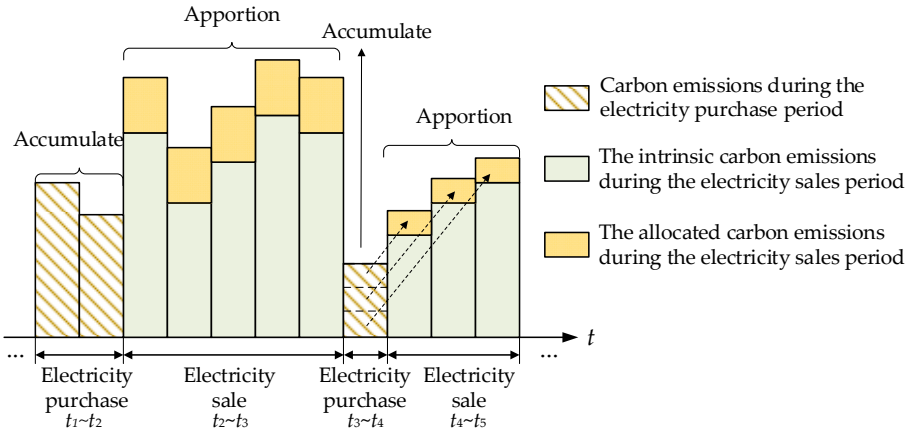


Figure 5. Accumulation–allocation of GH carbon emission.

Assuming t_1~t_2 is the electricity purchase interval of AP, and t_2~t_3 is the subsequent electricity sales interval. The accumulated carbon emissions during the purchase interval (t_1~t_2) are evenly distributed over the sales interval (t_2~t_3). The portion of the accumulated carbon emissions from the previous purchase interval allocated to each sales period is as follows:

$$R^{\text{att}}_{t,t\in[t_2,t_3]} = \frac{1}{N}\sum_{t\in[t_1,t_2]} R_{\text{vent},t}\Delta t \tag{23}$$

where R^{att}_t denotes the allocated carbon emission from the previous electricity purchase interval to the sales period. $R_{\text{vent},t}$ is the CO_2 emission rate from the GH during time period t ($kgCO_2/h$), and N is the number of time periods in the sales interval from t_2~t_3.

It should be specifically noted that any CO_2 emission of GH not allocated within the dispatch period is carried over in the form of initial accumulation and allocated during the first sales period of the following day. For the park's electricity sales period t, the carbon emission $R_{\text{GH},t}$ attached to the park's sales power is the sum of the emission R^{p2d}_t from the GH during that period and the allocated emission.

$$\begin{cases} R_{\text{GH},t} = R^{\text{p2d}}_t + R^{\text{att}}_t \\ R^{\text{p2d}}_t = R_{\text{vent},t}, \text{if } U_{\text{p2d},t} = 1 \\ R^{\text{att}}_t = \frac{1}{N_{\text{buy},t}}\sum_{t\in T_{\text{buy},t}} R_{\text{vent},t} \end{cases} \tag{24}$$

where $T_{\text{buy},t}$ denotes the electricity purchase interval preceding the sales interval for period t (where, if t falls in the t_2~t_3 interval, $T_{\text{buy},t} = [t_1, t_2]$; if t falls in the t_4~t_5 interval, $T_{\text{buy},t} = [t_3, t_4]$); $N_{\text{buy},t}$ is the total number of periods in the purchase interval $T_{\text{buy},t}$.

According to the principle of conservation of carbon emissions, carbon emissions during period t of park electricity sales satisfies the following balance relationship:

$$\rho_{\mathrm{p2d},t} P_{\mathrm{p2d},t} = \rho_t^{\mathrm{e}} P_{\mathrm{p2d},t} + U_{\mathrm{p2d},t} R_{\mathrm{GH},t} \tag{25}$$

where $\rho_{\mathrm{d2p},t}$ is the carbon intensity of the park's surplus electricity exported to the DN.

3. Stackelberg Game for Coordinated Scheduling of AP and DN

3.1. Bidirectional Carbon Tax Mechanism

The distribution network (DN), serving as an energy transmission network, is connected to the transmission grid and is equipped with distributed energy resources, such as PV, wind turbines, and gas/oil-fired generating units. The AP acts as a prosumer at the end of the DN. Except for PV and wind power, the remaining power sources in the DN, including the electricity exported from AP to DN, all have certain carbon densities, which affect the CEF distribution of the DN.

The 'bidirectional carbon tax' mechanism is based on the existing carbon tax mechanism [17]: on the base price of energy, add the 'carbon price' composed of the product of the carbon tax and the carbon intensity of energy, forming an energy–carbon integrated price. The higher the carbon intensity of energy, the higher the corresponding integrated price. This strategy encourages users to use cleaner energy. According to this, there are situations involving reverse power exports to the DN. The DN prefers that the AP export cleaner electricity to reduce its carbon cost. Thus, a reverse carbon tax mechanism is proposed. The integrated price of reverse power is inversely proportional to the carbon intensity. The higher the carbon intensity of the reverse electricity, the lower the integrated price. This way reduces the indirect carbon emissions of the electricity received by the DN from the AP. The 'bidirectional carbon tax' mechanism and the decision variables of the DN and AP are shown in Figure 6, where the arrows represent the directions of power flow and CEF.

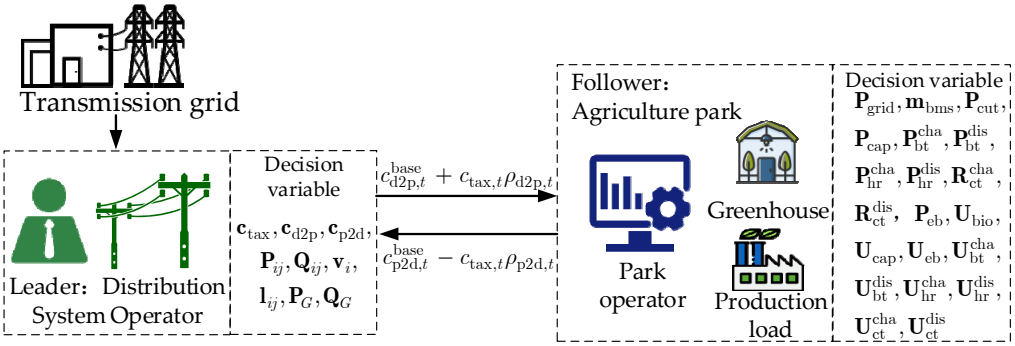


Figure 6. Pricing mechanism of bidirectional CEF (Decision variable explanation is at Section 3.4).

The calculation method for this 'reverse carbon intensity' takes into account the impact of carbon emission from terminal load GHs and is determined by the reverse carbon intensity calculation method proposed in Section 2.3. The DN pays the park for purchasing electricity based on the composite reverse electricity price. When the reverse carbon intensity is lower, the park's composite reverse electricity price is higher, thus incentivizing the AP to return low-carbon-intensity clean electric power to the DN.

Considering the bidirectional CEF with the electricity–carbon composite price, the proposed 'bidirectional carbon tax' can be summarized as follows:

$$\begin{cases} c_{\mathrm{d2p},t} = c_{\mathrm{d2p},t}^{\mathrm{base}} + c_{\mathrm{tax},t}\rho_{\mathrm{d2p},t} \\ c_{\mathrm{p2d},t} = c_{\mathrm{p2d},t}^{\mathrm{base}} - c_{\mathrm{tax},t}\rho_{\mathrm{p2d},t} \end{cases} \tag{26}$$

where $c_{\mathrm{d2p},t}^{\mathrm{base}}$ and $c_{\mathrm{d2p},t}$ are the base price and composite price for electricity sold by the DN to the park in period t, respectively; $c_{\mathrm{p2d},t}^{\mathrm{base}}$ and $c_{\mathrm{p2d},t}$ are the base price and composite price for electricity exported from AP to DN in period t, respectively; $c_{\mathrm{tax},t}$ is the carbon tax in period t; $\rho_{\mathrm{d2p},t}$ is the carbon intensity of the power sold by the DN in period t; $\rho_{\mathrm{p2d},t}$ is the carbon intensity of the power output by the park in period t.

A carbon tax in the existing literature is mostly based on empirical pricing, and it is a fixed value. Ref. [20] set it at 0.15 yuan/kg ('yuan' here is the unit of money in China). Under the current fluctuating situation of carbon prices in the carbon market, either excessively high or low carbon prices are not conducive to the interests of all parties and the promotion of carbon reduction (the sensitivity analysis experiment of the carbon tax is presented at Section 4.3.1). In this paper, carbon tax is regarded as a variable in the interaction of the game between DN and AP, and the optimal value of carbon tax between the two is determined by the Stackelberg game (details can be seen in Section 3.4 below).

3.2. Scheduling Model of AP

The park operator aims to minimize the cost as the objective function.

$$\begin{aligned} &\min C_{\mathrm{PO}} = \sum_{t=1}^{T}\left(C_{\mathrm{grid},t} + C_{\mathrm{bio},t} + C_{\mathrm{cut},t} + C_{\mathrm{ct},t} + C_{\mathrm{om},t} - C_{\mathrm{GH},t} - C_{\mathrm{L},t}\right) \\ &\begin{cases} C_{\mathrm{grid},t} = (c_{\mathrm{d2p},t}^{\mathrm{base}} + c_{\mathrm{tax},t}\rho_{\mathrm{d2p},t})P_{\mathrm{d2p},t} - (c_{\mathrm{p2d},t}^{\mathrm{base}} - c_{\mathrm{tax},t}\rho_{\mathrm{p2d},t})P_{\mathrm{p2d},t} \\ C_{\mathrm{bio},t} = c_{\mathrm{bio}}m_{\mathrm{bms},t} \\ C_{\mathrm{cut},t} = c_{\mathrm{cut}}P_{\mathrm{cut},t}\Delta t \\ C_{\mathrm{ct},t} = c_{\mathrm{ct}}(\rho_{\mathrm{bio}}P_{\mathrm{bio},t} - R_{\mathrm{cap},t} + R_{\mathrm{vent},t})\Delta t \\ C_{\mathrm{om},t} = \Big[c_{\mathrm{bt}}(P_{\mathrm{bt},t}^{\mathrm{cha}} + P_{\mathrm{bt},t}^{\mathrm{dis}}) + c_{\mathrm{hr}}(P_{\mathrm{hr},t}^{\mathrm{cha}} + P_{\mathrm{hr},t}^{\mathrm{dis}}) + c_{\mathrm{ctom}}(R_{\mathrm{ct},t}^{\mathrm{cha}} + R_{\mathrm{ct},t}^{\mathrm{dis}}) \\ \qquad +c_{\mathrm{CHP}}P_{\mathrm{CHP},t}^{\mathrm{e0}} + c_{\mathrm{cap}}P_{\mathrm{cap},t} + c_{\mathrm{ebom}}P_{\mathrm{eb},t}^{\mathrm{e}} + c_{\mathrm{pv}}P_{\mathrm{pv},t}\Big]\Delta t \\ C_{\mathrm{GH},t} = (c_{\mathrm{e},t}P_{\mathrm{GH},t}^{\mathrm{e}} + c_{\mathrm{h},t}P_{\mathrm{GH},t}^{\mathrm{h}} + c_{\mathrm{co_2}}R_{\mathrm{inj},t})\Delta t \\ C_{\mathrm{L},t} = (c_{\mathrm{e},t}P_{\mathrm{L},t}^{\mathrm{e}} + c_{\mathrm{h},t}P_{\mathrm{L},t}^{\mathrm{h}})\Delta t \end{cases} \end{aligned} \tag{27}$$

where C_{PO} is the total daily operational cost of the park. The detailed calculations of each cost and the explanations of the relevant variables are as follows.

The interaction cost $C_{\mathrm{grid},t}$ between the park and the DN, the interaction price of electricity is determined by the bidirectional carbon tax mechanism as (26). Specifically, the selling price of the AP is inversely proportional to the reverse carbon intensity. The reverse carbon intensity of the AP is calculated based on the CEF model proposed in Sections 2.2 and 2.3 of this paper, and then the reverse carbon tax mechanism is utilized to encourage the AP to return clean energy to the DN.

Fuel cost $C_{\mathrm{bio},t}$ and equipment operation and maintenance (O&M) cost $C_{\mathrm{om},t}$: c_{bio} is the fuel price of biogas CHP. The O&M cost is calculated based on the electric and thermal power of each energy device during time period t. The O&M cost coefficients for electric ES, heat ES, CHP unit, carbon capture device, electric boiler, and photovoltaic device are c_{bt}, c_{hr}, c_{CHP}, c_{cap}, c_{ebom} and c_{pv}, respectively. The O&M cost of the CO_2 storage tank is calculated based on the carbon flow rate during charging and discharging, with a cost coefficient of c_{ctom}. The curtailed solar penalty cost $C_{\mathrm{cut},t}$: $P_{\mathrm{pv},t}$ is the predicted maximum output power of photovoltaics during time period t, $P_{\mathrm{cut},t}$ is the curtailed power, and c_{cut} is

the cost coefficient. Carbon emission penalty cost $C_{ct,t}$: c_{ct} is the carbon emission penalty cost coefficient. Carbon emissions include both direct and indirect emissions within the park. Direct emission consists of CO_2 from CHP that is not captured and CO_2 emitted to the atmosphere through ventilation in the GH. The uncaptured CO_2 is represented by ($\rho_{bio}P_{bio,t} - R_{cap,t}$) (where ρ_{bio}, $P_{bio,t}$, and $R_{cap,t}$ are the biogas carbon intensity, total input energy to CHP, and carbon capture rate, respectively; see Equation (14)), and $R_{vent,t}$ is the CO_2 emission rate from the GH to the atmosphere. Indirect emission is reflected in the carbon emission responsibility the park incurs due to electricity purchases, which is calculated based on the carbon intensity $\rho_{d,t}$ at the park's connection node to the DN and the purchased power $P_{d2p,t}$, according to the CEF distribution in the DN.

The constraints of the AP include energy production/conversion equipment models: Equations (1)–(4); carbon capture system model and operational constraints: Equations (5)–(7); energy/CO_2 storage equipment models: Equations (8) and (9); electricity/heat/carbon balance constraints: Equation (10); and constraints on electricity interaction with the DN: Equations (11) and (12).

3.3. Dispatch Model and CEF Calculation of DN

The operational cost of the DN over a dispatching cycle is expressed as follows:

$$\begin{aligned} &C_{DSO} = \sum_{t=1}^{T} (C_{ep,t} + C_{obs,t} + C_{cet,t} + C_{ita,t} + C_{loss,t}) \\ &\begin{cases} C_{ep,t} = c_{tr,t}P_{tr,t} + c_{ess,t}P_{ess,t} + c_{pv}P_{dpv,t} + c_{g1}P_{g1,t} + c_{g2}P_{g2,t} + c_{wd}P_{wd,t} \\ C_{obs,t} = c_{pvc}(P_{pvm,t} - P_{dpv,t}) + c_{wdc}(P_{wdm,t} - P_{wd,t}) \\ C_{cet,t} = c_{ct}(\rho_{tr,t}P_{tr,t} + \rho_{g1}P_{g1,t} + \rho_{g2}P_{g2,t} + \rho_{p2d,t}P_{p2d,t}) \\ C_{ita,t} = (c_{p2d,t} - c_{tax,t})P_{p2d,t} - (c_{d2p,t} + c_{tax,t})P_{d2p,t} \\ C_{loss,t} = c_{loss}\sum_{ij\in B} l_{ij,t}P_{ij,t} \end{cases} \end{aligned} \tag{28}$$

where C_{DSO} represents the operational cost of the DN over a dispatching cycle. The expressions for each cost are as follows:

The electricity purchase cost of the DN $C_{ep,t}$: $P_{tr,t}$ is the power purchased from the higher-level grid, with $c_{tr,t}$ being the corresponding purchase price per unit; $P_{ess,t}$ is the charge/discharge power of the ES, and c_{ess} is the cost coefficient for energy loss during charge/discharge; $P_{dpv,t}$ and $P_{wd,t}$ are the power purchased from (PV) and wind power generation, respectively, with c_{pv} and c_{wd} being their respective cost coefficients; $P_{g1,t}$ and $P_{g2,t}$ are the power outputs from two small generator units (G1 and G2) within the DN, with c_{g1} and c_{g2} being their respective cost coefficients. Curtailed wind/solar penalty cost $C_{obs,t}$: $P_{pvm,t}$ and $P_{dpv,t}$ are the PV power generation and absorption, respectively. $P_{wdm,t}$ and $P_{wd,t}$ are the wind power generation and absorption, respectively. c_{pvc} and c_{wdc} are the cost coefficients for curtailed solar and wind power, respectively.

Carbon emission penalty cost $C_{cet,t}$ and network loss cost $C_{loss,t}$: $\rho_{tr,t}$ is the carbon intensity of the power $P_{tr,t}$ purchased from the higher-level grid, and ρ_{g1} and ρ_{g2} are the carbon densities of the power generated by G1 and G2, respectively. c_{loss} is the cost coefficient for network loss. Cost of interaction with the AP $C_{ita,t}$: $P_{p2d,t}$ is the surplus power exported from AP to DN, $\rho_{p2d,t}$ is the carbon intensity of the surplus power exported from AP to DN, $c_{p2d,t}$ is the unit price of the surplus power exported from AP to DN, $c_{d2p,t}$ is the unit price of electricity sold by the DN to AP, and $c_{tax,t}$ is the carbon tax.

The DN employs the Distflow model and second-order cone constraints to characterize the branch power flow relationships [29]:

$$\begin{cases} \sum\limits_{k:j\to k} P_{jk,t} = \sum\limits_{i:i\to j} (P_{ij,t} - l_{ij,t} r_{ij}) - (P_{Gj,t} - P_{Lj,t}) \\ \sum\limits_{k:j\to k} Q_{jk,t} = \sum\limits_{i:i\to j} (Q_{ij,t} - l_{ij,t} x_{ij}) - (Q_{Gj,t} - Q_{Lj,t}) \\ v_{j,t} = v_{i,t} - 2(r_{ij} P_{ij,t} + x_{ij} Q_{ij,t}) + (r_{ij}^2 + x_{ij}^2) l_{ij,t} \\ 4{P_{ij,t}}^2 + 4{Q_{ij,t}}^2 + (l_{ij,t} - v_{i,t})^2 \le (l_{ij,t} + v_{i,t})^2 \end{cases} \tag{29}$$

where $P_{jk,t}$ and $P_{ij,t}$ are the active power from node j to node k and from node i to node j, respectively. $Q_{jk,t}$ and $Q_{ij,t}$ are the corresponding reactive power. $P_{Gj,t}$ and $P_{Lj,t}$ are the active power injection and load at node j. $Q_{Gj,t}$ and $Q_{Lj,t}$ are the reactive power injection and load. $l_{ij,t}$ is the squared current in the line, and $v_{i,t}$ is the squared voltage at the node.

The DN also needs to satisfy constraints on node voltage, branch current, generator output, and branch power flow:

$$\begin{cases} v_{i,\min} \le v_{i,t} \le v_{i,\max},\ l_{i,\min} \le l_{i,t} \le l_{i,\max},\ P_{ij,t} < P_{\mathrm{B},\min} \\ P_{G,\min} \le P_{G,k} \le P_{G,\max},\ Q_{G,\min} \le Q_{G,k} \le Q_{G,\max} \end{cases} \tag{30}$$

where $v_{i,\min}$ and $v_{i,\max}$ are the squared minimum and maximum node voltages, respectively; $l_{i,\min}$ and $l_{i,\max}$ are the squared minimum and maximum branch currents, respectively; $P_{\mathrm{B},\min}$ is the minimum branch power flow; $P_{\mathrm{G},k}$ and $Q_{\mathrm{G},k}$ are the active and reactive power outputs of generator k; $P_{\mathrm{G},\min}$, $P_{\mathrm{G},\max}$, $Q_{\mathrm{G},\min}$, and $Q_{\mathrm{G},\min}$ are the minimum and maximum active and reactive power outputs of the generator.

The nodal carbon intensity in the system is calculated based on the power flow distribution results of the DN as follows [30]:

$$e_{Ni} = \frac{\sum\limits_{s\in S^+} P_{\mathrm{B},s}\rho_s + P_{\mathrm{G},i} e_{\mathrm{G}i}}{\sum\limits_{s\in S^+} P_{\mathrm{B},s} + P_{\mathrm{G},i}} \tag{31}$$

where s is a branch from the upstream branch set $S+$, $P_{\mathrm{B,s}}$ is the power flow of the upstream branch, and ρ_{s} is the carbon intensity of the power flow entering node i through branch s.

Additionally, the CEF calculation for ES in the DN is consistent with that in the AP.

3.4. Stackelberg Game Model and Algorithm

In the scenario described in this article, there is a hierarchical relationship of decision-making between DN and AP. The DN has greater market influence and decision-making priority, and thus assumes the role of a leader, while the AP needs to respond based on the decisions made by the DN, taking on the role of a follower. The Stackelberg game theory as a dynamic game is inherently applicable to the structure and can depict the strategic interaction between the leader and the follower. The model of the Stackelberg game proposed in this chapter can be described as follows:

$$G = \{\mathrm{DSO} \cup (\mathrm{PO}), \{S_{\mathrm{DSO}}\}\{S_{\mathrm{PO}}\}, \{C_{\mathrm{DSO}}\}, \{C_{\mathrm{PO}}\}\} \tag{32}$$

In the game model G, the participants include the distribution system operator (DSO) and the park operator (PO). The DSO acts as the leader, who has the authority to set and issue electricity purchase and sale prices as well as carbon taxes. The PO acts as the follower, who formulates its own dispatch and operation plan based on the electricity prices and carbon tax information issued by the DSO.

The strategy set S_{DSO} of the DSO and S_{PO} of PO corresponds to the decision variables of the DSO and PO dispatch model:

$$\begin{cases} S_{\mathrm{DSO}} = \left\{ \mathbf{c}_{\mathrm{tax}}, \mathbf{c}_{\mathrm{d2p}}, \mathbf{c}_{\mathrm{p2d}}, \mathbf{P}_{ij}, \mathbf{Q}_{ij}, \mathbf{v}_i, \mathbf{l}_{ij}, \mathbf{P}_G, \mathbf{Q}_G \right\} \\ S_{\mathrm{PO}} = \left\{ \mathbf{P}_{\mathrm{grid}}, \mathbf{m}_{\mathrm{bms}}, \mathbf{P}_{\mathrm{cut}}, \mathbf{P}_{\mathrm{cap}}, \mathbf{P}_{\mathrm{bt}}^{\mathrm{cha}}, \mathbf{P}_{\mathrm{bt}}^{\mathrm{dis}}, \mathbf{P}_{\mathrm{hr}}^{\mathrm{cha}}, \mathbf{P}_{\mathrm{hr}}^{\mathrm{dis}}, \mathbf{R}_{\mathrm{ct}}^{\mathrm{cha}}, \mathbf{R}_{\mathrm{ct}}^{\mathrm{dis}}, \right. \\ \qquad \left. \mathbf{P}_{\mathrm{eb}}, \mathbf{U}_{\mathrm{bio}}, \mathbf{U}_{\mathrm{cap}}, \mathbf{U}_{\mathrm{eb}}, \mathbf{U}_{\mathrm{bt}}^{\mathrm{cha}}, \mathbf{U}_{\mathrm{bt}}^{\mathrm{dis}}, \mathbf{U}_{\mathrm{hr}}^{\mathrm{cha}}, \mathbf{U}_{\mathrm{hr}}^{\mathrm{dis}}, \mathbf{U}_{\mathrm{ct}}^{\mathrm{cha}}, \mathbf{U}_{\mathrm{ct}}^{\mathrm{dis}} \right\} \end{cases} \tag{33}$$

All the above variables are 1×24 column vectors, corresponding to the decision variables for the 24 time periods in the day-ahead dispatch (the follower's decision variables are similar). $\boldsymbol{c}_{\mathrm{tax}}$ is carbon tax; $\boldsymbol{c}_{\mathrm{d2p}}$ and $\boldsymbol{c}_{\mathrm{p2d}}$ are sale and selling price of the DN; $\boldsymbol{P}_{ij}$ and $\boldsymbol{Q}_{\mathrm{ij}}$ are power flow of the DN; $\boldsymbol{v}_i$ and $\boldsymbol{l}_{\mathrm{ij}}$ are square of nodal voltage and branch current. $\boldsymbol{P}_{\mathrm{grid}}$ is power interaction between DN and AP; $\boldsymbol{m}_{\mathrm{bms}}$ is the mass of biomass material; $\boldsymbol{U}_{\mathrm{bio}}$ is the binary; $\boldsymbol{P}_{\mathrm{cut}}$ and $\boldsymbol{P}_{\mathrm{cap}}$ are power of curtailed PV and carbon capture device; $\boldsymbol{U}_{\mathrm{cap}}$ is the binary; $\boldsymbol{P}_{\mathrm{eb}}$ and $\boldsymbol{U}_{\mathrm{eb}}$ are boiler power and the binary. $\mathbf{P}_{\mathrm{bt}}^{\mathrm{cha}}, \mathbf{P}_{\mathrm{bt}}^{\mathrm{dis}}, \mathbf{P}_{\mathrm{hr}}^{\mathrm{cha}}, \mathbf{P}_{\mathrm{hr}}^{\mathrm{dis}}, \mathbf{R}_{\mathrm{ct}}^{\mathrm{cha}}, \mathbf{R}_{\mathrm{ct}}^{\mathrm{dis}}$ are the charging/release power/rate of ES, and $\mathbf{U}_{\mathrm{bt}}^{\mathrm{cha}}, \mathbf{U}_{\mathrm{bt}}^{\mathrm{dis}}, \mathbf{U}_{\mathrm{hr}}^{\mathrm{cha}}, \mathbf{U}_{\mathrm{hr}}^{\mathrm{dis}}, \mathbf{U}_{\mathrm{ct}}^{\mathrm{cha}}, \mathbf{U}_{\mathrm{ct}}^{\mathrm{dis}}$ are the binary, respectively. The strategy set represents the decision variables of the park dispatch model.

The utilities of DSO and PO are C_{DSO} and C_{PO}, respectively, which correspond to the objective functions of their respective dispatch models, as shown in Equations (27) and (28). For a given strategy profile (S_{DSO}^*, S_{PO}^*), if the following conditions are satisfied, then this strategy profile is a Nash equilibrium solution of the game model.

$$\begin{cases} C_{\mathrm{DSO}}^*\left(S_{\mathrm{DSO}}^*, S_{\mathrm{PO}}^*\right) \le C'_{\mathrm{PO}}\left(S_{\mathrm{DSO}}, S_{\mathrm{PO}}^*\right) \\ C'^*_{\mathrm{PO}}\left(S_{\mathrm{DSO}}^*, S_{\mathrm{PO}}^*\right) \le C'_{\mathrm{PO}}\left(S_{\mathrm{DSO}}^*, S_{\mathrm{PO}}\right) \end{cases} \tag{34}$$

Particle swarm optimization (PSO) is suitable for addressing the interactive process of the Stackelberg game by low algorithmic complexity and fast convergence rate. Particles in PSO dynamically adjust their positions based on individual experience (personal best position) and collective experience (global best position) to progressively approach the optimal solution. The Algorithm 1 is as follows.

The proposed algorithm is also applicable to solving the carbon–energy coordinated dispatch problem between the AP and the DN under the following scenarios: x (1) When CEF is not considered, the carbon tax is set to zero in the algorithm. In steps (i) and (ii), the 'carbon information' exchanged between the DN and the AP is changed from 'carbon intensity' to 'carbon emission factor'. (2) When only the unidirectional CEF on the DN side is considered, the carbon tax on reverse power is set to zero in the algorithm. In step (ii), the carbon intensity of reverse power exported from the AP to the DN is changed to 'carbon emission factor'. (3) When considering the dispatch with bidirectional CEF, the carbon accounting cost method of the AP and DN bearing the indirect carbon emission from electricity purchase is adopted. In the algorithm, the carbon tax is set to zero, and the carbon cost items of the two entities correspondingly change in steps (ii) and (iii).

Algorithm 1 PSO Algorithm for Stackelberg Game

1. Input the basic data of the DN and the AP (including the fundamental model data, meteorological forecast data, time-of-use electricity prices and carbon intensity information of transmission grid, etc.), the basic data of the PSO algorithm (comprising the swarm size M, the maximum iterations $k_{\max}$, inertia weight, individual and social learning factors, etc.), and the initial predicted power interaction and carbon intensity information for electricity between the AP and the DN $P_{\mathrm{grid},t}$ and $\rho_{\mathrm{p2d},t}$.

Algorithm 1 *Cont.*

2. Initialize the particle swarm by randomly generating M particles, with the basic purchase/sale electricity prices $c_{\mathrm{d2p},t}^{\mathrm{base}}$, $c_{\mathrm{p2d},t}^{\mathrm{base}}$ and the carbon tax $c_{\mathrm{tax},t}$ of the DN serving as the attributes of each particle.
3. Initialize the outer iteration counter $k = 1$.
4. If $k < k_{\max}$, execute the following steps iteratively:
   (1) The DN formulates M sets of electricity–carbon prices for interaction with the AP based on the current nodal carbon intensity and the interaction power and carbon intensity from the AP, according to Equation (26).
   (2) Complete the low-carbon optimal dispatch of the park under M sets of purchase/sale electricity–carbon integrated prices, obtain M sets of park dispatch plans, and report the corresponding electricity purchase/sale power and reverse carbon intensity of the M sets of dispatch plans to the DN.
   (3) The DN completes the low-carbon economic dispatch based on the M sets of purchase/sale electricity–carbon integrated prices and the corresponding interaction power and carbon intensity ($P_{\mathrm{grid},t}$ and $\rho_{\mathrm{p2d},t}$) exported from AP to DN after the game equilibrium, according to Equation (28). Based on the obtained power flow of the DN, the carbon intensity results for each time period and each node within the DN cycle are obtained by Equation (31).
   (4) Update the individual and global best values and their corresponding objective function values for each particle in the M sets.
   (5) Using the DN operational cost as the fitness function $F_{\mathrm{DSO}(k)}$, update the particle swarm based on the individual and global best values from the previous step, inertia weight, and learning factors to form a new generation of particles.
5. Output the Stackelberg equilibrium solution for the DN and the AP.

4. Case Study

4.1. Simulation Setup

The IEEE 33-bus distribution network and an AP connected at bus 24 are employed as case studies to validate the effectiveness of the proposed CEF model for APs and the bidirectional carbon tax mechanism. The topology of the distribution network, distributed energy resources, and AP interconnections are illustrated in Figure 7.

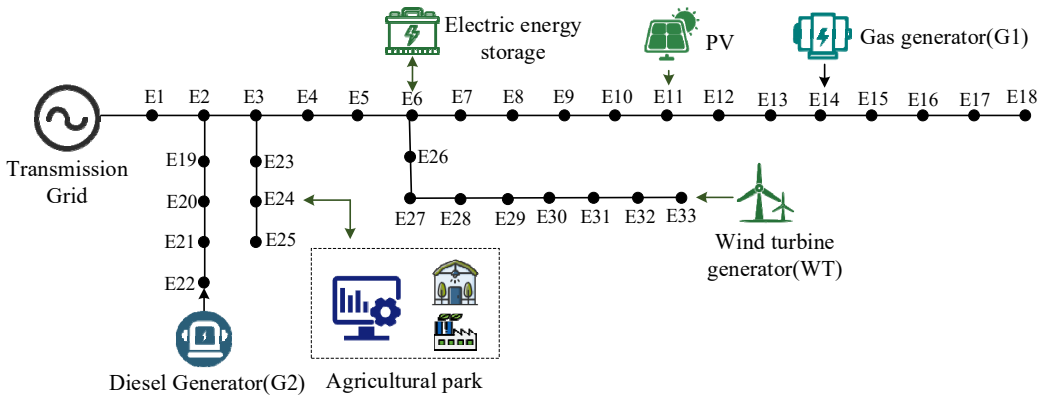


Figure 7. Topology diagram of the test system.

The distribution network (DN) is connected to the transmission grid via slack bus E1. An energy storage (ES) system is installed at bus E6 to mitigate power fluctuations from intermittent renewable sources and enhance dispatch flexibility. A photovoltaic unit is located at bus E11, while gas-fired (G1) and diesel-fueled (G2) generation units are situated at buses E14 and E22, respectively. Wind power is integrated at bus E33. Detailed network and AP parameters are provided in the Data Availability Statement. The transmission grid's time-of-use pricing periods are valley (23:00–07:00), flat (08:00–10:00, 15:00–17:00), and peak (11:00–14:00, 18:00–23:00).

The particle swarm optimization (PSO) algorithm is configured with a swarm size of 30, maximum iterations of 40, inertia weight of 0.7, and individual/global learning factors of 1.5. The scheduling models for the DN and AP are implemented in MATLAB R2023a, formulated using YALMIP 1.1, and solved with the GUROBI 12.0 solver.

As indicated in Figure 8, the greenhouse necessitates the park to supply electrothermal energy and has CO_2 demands and emissions. It also includes other agricultural production loads with electrothermal energy requirements. The greenhouse's primary load characteristics are as follows: (1) Supplementary lighting is required at the day–night junction, resulting in high electricity during this consumption period. (2) The thermal load is lower during the day than at night due to the photovoltaic thermal effect. (3) Crop photosynthesis within the greenhouse generates daytime-only carbon demand, while ventilation causes CO_2 escape (carbon emission). The carbon emission level is lower than the carbon demand, indicating the greenhouse's 'carbon sink' attribute. For other agricultural production loads, electricity demand is predominant in the daytime, while thermal demand peaks in the morning and evening.

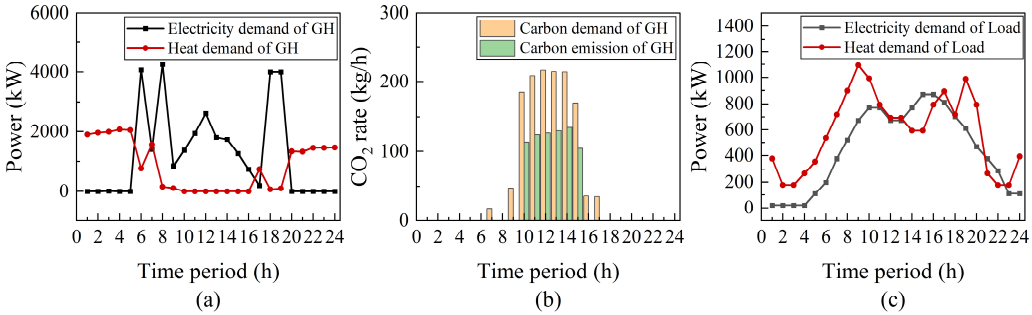


Figure 8. The energy/resources requirements of the park users: (**a**) Electricity/Heat demand of GH; (**b**) CO_2 demand/emission of GH; (**c**) Electricity/Heat demand of the Loads.

4.2. CEF Results of AP

4.2.1. Carbon Intensity of the Electrical/Heat Power Supplied to Park Users

This section analyzes the carbon emission factor (CEF) associated with specific energy flows in the park, as depicted in Figure 9. Figure 9a illustrates the electricity output and carbon intensity of the combined heat and power (CHP) unit. During daytime, abundant photovoltaic (PV) generation reduces CHP output, resulting in lower carbon intensity compared to nighttime. This is attributed to the greenhouse's CO_2 demand, which maximizes carbon capture and reduces CHP carbon intensity. Figure 9b shows the combined electricity supply and carbon intensity from PV/CHP units and the distribution network. The high daytime PV generation proportion results in near-zero carbon intensity. In Figure 9c, the carbon intensity of electricity discharged from the electrical energy storage (ES) system increases slightly after charging at hour 8, decreases at hour 10 due to daytime PV charging, and approaches zero after hour 15. Figure 9d presents the carbon intensity of electricity consumption by park loads, which is near-zero between hours 9 and 16 and higher (around

0.5) in the early morning and night. The decrease at hours 18 and 19 is due to the ES system discharge of daytime-stored clean energy.

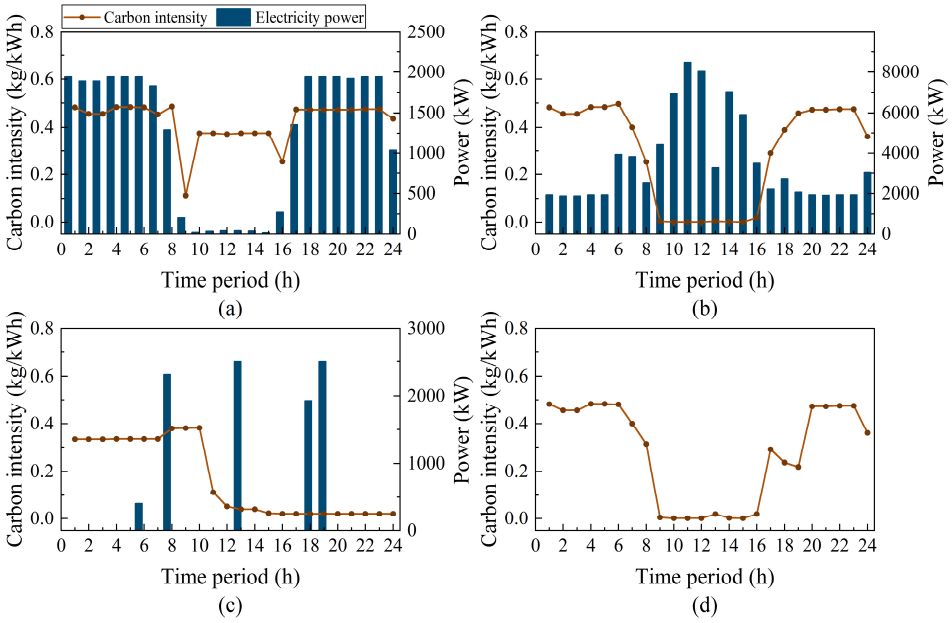


Figure 9. Distribution of electricity and CEF in the park: (**a**) CHP electricity generation and carbon intensity; (**b**) Integrated CHP/PV/DN electricity and carbon intensity; (**c**) Electric ES discharge and carbon intensity; (**d**) Carbon intensity of electricity consumption in the park's load.

The carbon intensity of thermal energy is shown in Figure 10.

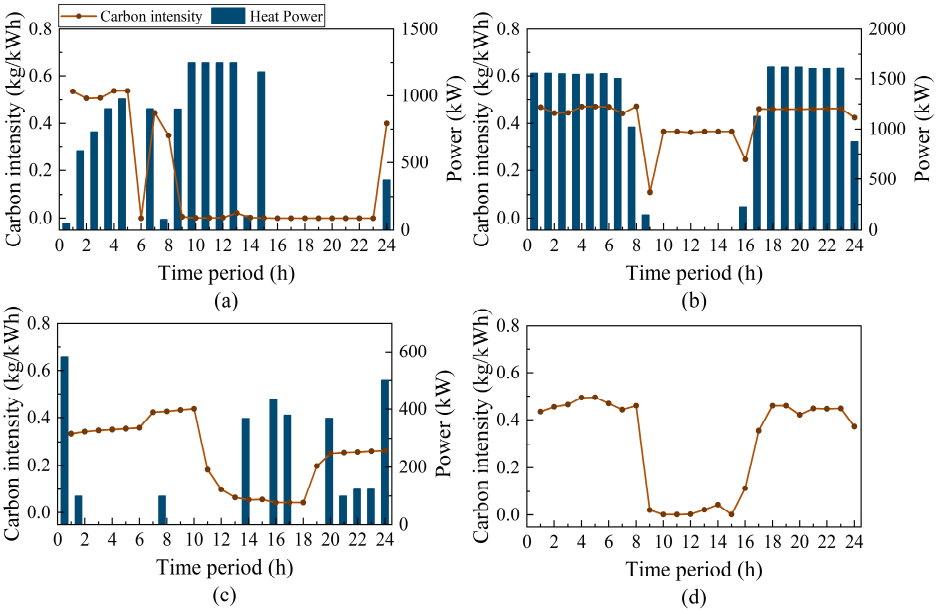


Figure 10. Distribution of heat and its carbon flows in the park: (**a**) Electric boiler heat generation and carbon intensity; (**b**) CHP heat production and carbon intensity; (**c**) Heat release and carbon intensity of heat ES (**d**) The heat carbon intensity of the load in the park.

When the electric boiler is out of operation, its carbon intensity is zero. During the day, the electric boiler operates at full capacity, converting excess clean electricity into heat. The distribution of heat output and carbon intensity from the CHP unit resembles that of its electricity generation. The thermal ES charges during the day, and reduces its discharging carbon intensity, but after storing heat at night, its carbon intensity increases. Figure 10d

presents the overall carbon intensity of heat supply from the electric boiler, CHP unit, and thermal ES. Similar to the carbon intensity of electricity, it is low between 9:00 and 15:00 and higher during other periods.

4.2.2. Carbon Intensity of Power Exported from AP to DN

As outlined in Section 2.3, when the park interacts with the distribution network, the carbon intensity of the electricity exported from AP to DN must account for the greenhouse carbon emissions. This section presents the applicability of the carbon density results of the park's feed-back power under different photovoltaic output scenarios. Figure 11a shows the interaction power results between DN and AP. Figure 11b demonstrates the impact of greenhouse carbon emissions on the carbon density of the park's feed-back electricity. Figure 11c presents the carbon density results of electricity consumption within the park and external power transmission when the photovoltaic power is insufficient. Emissions of GH are allocated to the corresponding power generation periods following the method in Figure 5.

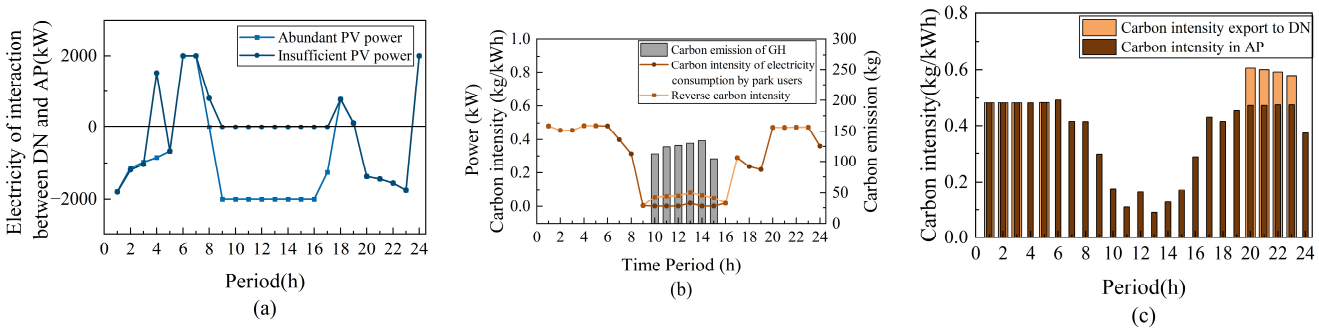


Figure 11. (**a**) Power exchange between AP and the DN under abundant/insufficient PV power; (**b**) Emission of GH and carbon intensity of power supply in AP/reverse to DN when PV power is abundant; (**c**) Carbon intensity for power supply in AP/reverse to DN when PV power is insufficient.

When the park purchases electricity from the distribution network, the carbon intensity of the park's load consumption is determined by the carbon intensity of the purchased grid electricity. Conversely, when the park sells surplus electricity back to the grid, the carbon intensity of energy used by park consumers is solely determined by internal energy devices. However, the carbon intensity at the grid node is influenced by greenhouse carbon emissions, specifically incorporating emissions from the park's greenhouses into the carbon intensity calculation of exported electricity. During periods when surplus electricity is exported from the AP to the DN, the carbon intensity of this surplus electricity is higher than that of the electricity used within the park during daytime, due to the inclusion of greenhouse emissions.

4.3. Effectiveness Analysis of Bidirectional Carbon Tax Mechanism

To verify the effectiveness of introducing CEF for low-carbon coordination between AP and DN, and to demonstrate the advantages of the bidirectional carbon tax mechanism proposed in this paper that considers bidirectional CEF, several coordinated cases between DNs and APs are compared in Table 1. All four cases adopt a game-theoretic approach for energy/price interaction.

Table 1. Setting of the four cases.

Case	CEF	Interacted 'Carbon' Information Between DSO and PO
1	Neglected	Both transmit 'carbon emission factor'
2	Unidirectional	DSO transmits carbon intensity, PO transmits 'carbon emission factor'
3	Bidirectional	Both transmit carbon intensity, DSO and PO accounting for carbon emission based on carbon intensity like [17]
4	Bidirectional	Both transmit carbon intensity, DSO guides the park's purchase/sale of clean electricity through bidirectional carbon taxes.

Case 1: CEF is neglected. Both the park and the distribution network use the average carbon emission factor as the interactive information of carbon. The DN takes the unified carbon emission factor of each node in the whole dispatching cycle as the boundary information to be sent to the AP. The park reports a 'generation carbon emission factor' to the distribution network, calculated as total carbon emission divided by generation output. Both parties conduct low-carbon scheduling based on this factor.

Case 2: Only the CEF of the DN is considered. Following the method of ref. [25], the distribution network calculates the CEF distribution across different nodes and periods. It then issues purchase-sale electricity prices and carbon intensity information for the park's connection node to the park. The park reports the 'generation carbon emission factor' to the distribution network. The park and the distribution network, respectively, bear the carbon tax (constant) when purchasing electricity and calculate the low-carbon scheduling of carbon emission to complete the interaction between the two sides.

Case 3: Bidirectional CEFs are considered. The park calculates the carbon intensity of surplus electricity exported from AP to DN using the proposed method and reports it to the distribution network, considering its impact on the DN. Drawing on the approach in [17], indirect carbon emission is calculated based on exchanged electricity and carbon intensity info. Carbon emission costs are incorporated into the costs of both the DN and the park. This enables low-carbon coordination between them.

Case 4: The case proposed in this paper. The carbon/energy interaction information is consistent with Case 3, but the bidirectional carbon tax mechanism proposed in this paper is adopted to encourage the purchase/sale of clean energy in the park.

4.3.1. Sensitivity Analysis of Carbon Tax

We conducted a comparative test using the different determination methods of carbon tax under the bidirectional carbon tax mechanism of Case 4 and analyzed the interaction results of AP and DN under different carbon tax values.

In Figure 12a, it can be seen that as the carbon tax increases, the cost of DSO decreases, while the cost of AP increases (revenue decreases). This is because a higher carbon tax is beneficial for the leader to charge electricity fees by setting higher prices. However, the carbon emissions of both parties do not decrease linearly with the increase in the carbon tax. An excessively high carbon tax affects trading enthusiasm and makes it difficult to achieve the optimal carbon emissions.

It can be seen that the current fixed carbon tax is unable to achieve the optimal situation for the transaction between the two parties. Therefore, this paper adopts a game theory approach to determine the carbon tax between AP and DSO. After the interaction between the DN and the AP in Case 4 reaches equilibrium, the results of the purchase and sale price and the bidirectional carbon tax formulated by the DN are shown in Figure 12b.

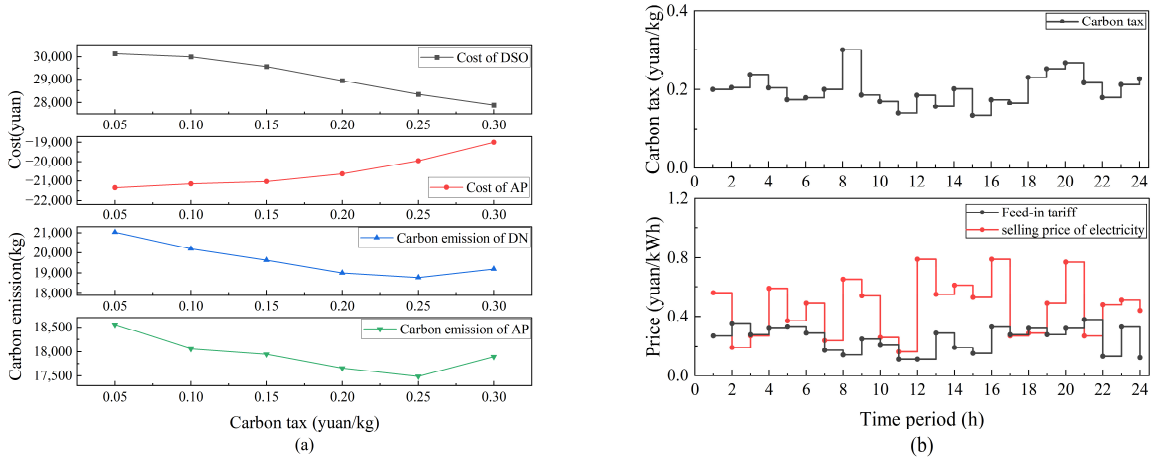


Figure 12. (**a**) The costs and carbon emission results of AP and DN under the sensitivity of carbon tax and (**b**) Purchase and sale prices and the carbon tax results of DN under the game mode.

The price difference between the nighttime and the daytime is different. The daytime price difference is large, and the nighttime price difference is small, indicating that the DN encourages the park to sell more clean energy power during the day. Carbon tax is at a low level during the daytime when the park's carbon intensity is relatively low, indicating that the DN can encourage the park to return clean energy power through the carbon tax in different periods.

4.3.2. Comparative Analysis of Four Cases

1. Cost Comprehensive Analysis of four cases

Table 2 shows the results of costs and carbon emission after the interaction between the AP and the DN reaches equilibrium under the four cases.

Table 2. Operating cost (yuan) and emission (kg) under four cases.

Case	1	2	3	4
Total cost of DSO	30,527.3	30,191.7	29,972.6	28,136.9
Power purchase cost of DSO	15,666.3	16,932.9	16,628.7	17,425.8
Cost interacting with PO	8535.6	7018.2	7512.7	4972.2
Network loss cost of DSO	1259.0	1240.5	1253.7	1234.0
Total cost of PO	−21,366.7	−21,814.1	−21,112.4	−20,375.4
PV curtailment cost of PO	217.0	204.1	125.6	115.7
Carbon emission of DSO	21,586.2	21,254.5	19,141.5	18,778.5
Carbon emission of DSO from PO	10,471.1	7199.2	6279.4	4102.8
Carbon emission of PO	19,644.0	18,343.5	18,003.0	17,317.5

As shown in Table 2, The park's costs and carbon emissions, as well as its greenhouse and production loads, decreased from Case 1 to Case 4. Specifically, compared to Cases 1–3, DN cost in Case 4 decreased by 7.8%, 6.8%, and 6.1%, respectively, while the carbon emission cost decreased by 13.0%, 11.6%, and 4.4%. Although the park cost increased by 3.1%, 3.6%, and 2.7% relative to Cases 1–3, the carbon emission reductions (11.8%, 5.6%, and 3.8%) exceeded the cost increases. This suggests that the park's partial economic trade-off enhances its environmental performance. In Case 4, the proposed mechanism

effectively conveyed the carbon intensity of electricity from the park to the DN, resulting in cleaner electricity transmission and significant carbon emission reductions. Moreover, the proposed mechanism optimized the DN's loss cost and the curtailed cost.

As shown in Figure 13, the interaction power between the DN and the AP after reaching equilibrium for Cases 1 to 4 is presented, along with the carbon intensity of electricity dispatched from the park to the grid and the nodal carbon intensity of the DN when the park purchases electricity, considering the bidirectional CEF.

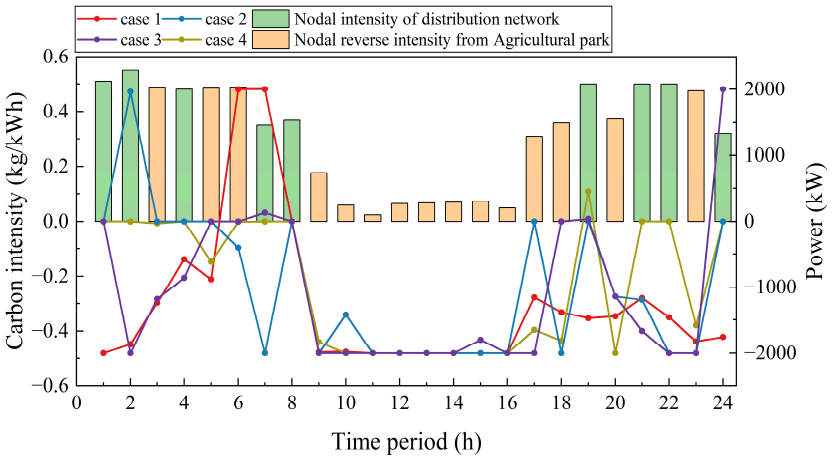


Figure 13. Carbon and energy interaction information between DN and AP.

In Case 1, the park sends electricity back to the grid during hours 1–5 and buys much electricity from the grid during hours 6–7. From hours 1–5, due to insufficient PV output, the park uses biogas CHP and electric ES for power, which have a high carbon intensity. This raises the grid's carbon emission when this electricity is sent back. During hours 6–8, the grid's carbon intensity is high, so buying much electricity causes the park to bear high indirect carbon emissions from power purchases. In this paper's CEF case, the park only sends electricity to the grid during hour 5 and does not purchase electricity from the grid during hours 6–7, lessening the carbon emission impact on both sides. Also, in Case 1, the park often sends electricity back to the grid at night, creating more carbon emissions for the grid. Compared with Case 1, the purchase and sale power and period of Case 2 are changed, the total power sold in the park is reduced, and the DN reduces the interaction cost with the park by mastering the way of setting the purchase and sale price.

Compared to Case 2, Case 3 prioritizes exporting power to the DN during the daytime and shifts power purchases from early morning to nighttime. Case 4 further reduces electricity exports to the DN during high-carbon periods in the morning and night (except hour 5), resulting in eight periods with no power interaction. Power purchases from the DN are minimal, occurring only in hour 19, while exports are concentrated during daytime periods with abundant photovoltaic generation. This strategy significantly reduces indirect carbon emissions from transmission and interaction costs between AP and DN.

2. Comparison of Case 1, 2 and 4

Compared to Case 1, Case 2 reduces the DN cost by 335.6 yuan and carbon emission by 331.7 kg, while increasing the park operator's revenue by 447.4 yuan and reducing carbon emission by 1301 kg. Case 1 employs a static carbon emission factor (CEF) without considering dynamic CEF, which is detrimental to both economic and low-carbon objectives. In Case 2, the DN utilizes unidirectional CEF to guide the park's energy interactions, reducing interaction costs and total DN expenses. However, both Cases 1 and 2 use a uniform park CEF, failing to capture temporal variations in carbon intensity. This limits the DN's ability to account for carbon emissions during energy interactions with the park.

As illustrated in Figure 14, during early morning valley periods, both Case 1 and Case 4 involve DN purchases from the main grid, with minimal ES charging. However, the high carbon intensity of main grid electricity during this period leads to increased DN carbon emissions in Case 1 due to substantial electricity purchases to meet park load demands. In contrast, Case 4 reduces DN carbon emissions through lower electricity purchases. During daytime, Case 4 maximizes PV output and ES charging for later discharge. At night, Case 1 requires significant electricity purchases and high generator output to meet peak loads, while Case 4 reduces both, lowering overall DN carbon emissions.

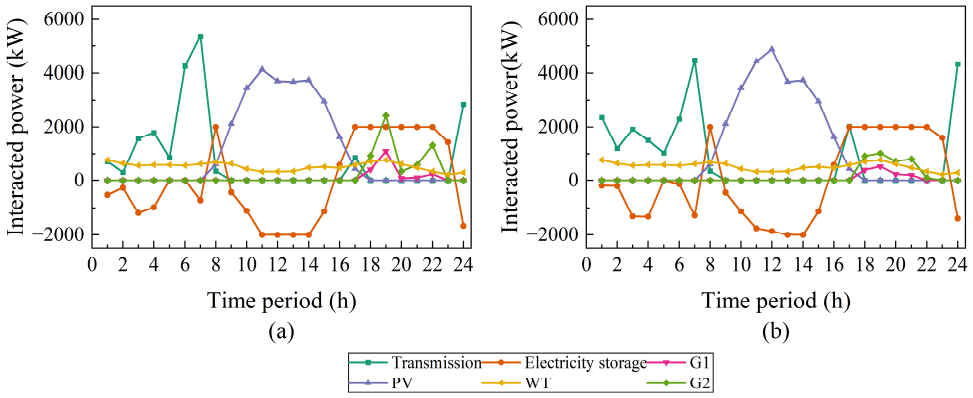


Figure 14. Output of generating units in DN: (**a**) Case 1; (**b**) Case 4.

3. Comparison of Case 2, 3 and 4

The CEF results of the DN of Cases 2 to 4 are shown in Figure 15. During the daytime, the abundant power of PV results in low carbon intensity across nodes in all three cases. Within the same period, a node's carbon intensity is influenced by its generators and incoming carbon emission, leading to varying carbon densities among nodes.

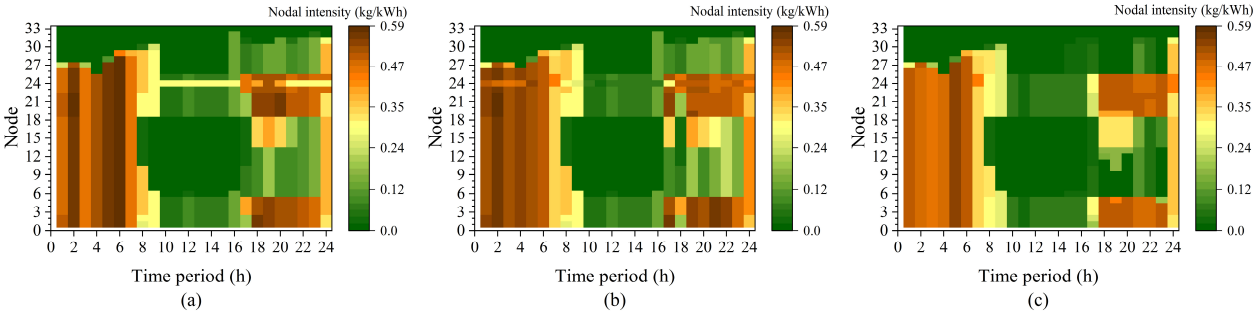


Figure 15. (**a**)–(**c**): The carbon intensity heatmaps of DN Cases 2~4.

During hours 6 and 7, Case 2 exhibits significantly higher carbon intensity than Case 4 due to electricity exports from the park to the DN without PV generation, as shown in Figure 13. Hours 1 to 27 have high carbon intensity, while subsequent periods, supported by wind power, approach near-zero carbon intensity. In later periods, reduced electricity exports and lower generator output in Case 4 lower the DN's carbon intensity compared to Case 2. In Case 2, the park considers only a static CEF as a 'power source', with limited unidirectional CEF interaction between the DN and the park. The park's power transmission has uniform carbon intensity across periods, despite surplus electricity in the AP. The DN passively accepts electricity and carbon emissions at a fixed carbon price, without perceiving the impact of varying on-grid carbon densities on DN emissions.

In Case 3, the bidirectional CEF between the park and the DN is considered, enabling full utilization of CEF information from both sides. With precise knowledge of the carbon

intensity of returned power in each period, the DN can optimize its operational cost and carbon emissions by balancing the impacts of power purchase costs and carbon costs. The DN's CEF results in Case 3 are illustrated in Figure 15b. During hours 1–4 and 20–23, power transmission from the park to the DN results in higher carbon intensity for the DN.

From a cost and carbon emission perspective, Case 4 reduces the DN cost by 1835.7 yuan compared to Case 3, with the interaction cost decreasing by 2540.5 yuan (a 34% reduction). This is primarily due to the DN's reduced power purchases from the park during high-carbon periods, resulting in a 35% decrease in indirect carbon emissions (2176.6 kg). In Case 3, the DN utilizes the AP's CEF solely for carbon emission calculation, treating carbon costs as a fixed component in low-carbon scheduling. Consequently, other costs such as energy and operation and maintenance expenses dominate the DN's objectives. This CEF-based carbon accounting mechanism fails to effectively guide the park to return clean energy to the DN, limiting the reduction of the park's impact on the DN's low-carbon goals.

In Case 4, the power purchase cost of the DN is higher than that of Case 3, and the interaction cost with the park and the carbon emission of the park to the DN is significantly reduced. The designated purchase and sale price of the DN and the bidirectional carbon tax results are shown in the previous part. The bidirectional carbon tax mechanism is used in Case 4, and the reverse carbon tax method, which is proportional to the carbon intensity of the park, is used to punish the carbon tax in the basic electricity price of the network. The higher the carbon intensity is, the higher the carbon price is, and the lower the corresponding energy–carbon price is, which achieves the guiding role of the park to send clean electricity back to the DN.

Based on the analysis, the carbon emissions from the park to the DN in Case 4 are reduced by 60.8%, 43.0%, and 34.7%, respectively, compared with Cases 1–3. The carbon emission of the park is reduced, and the DN achieves a double reduction in cost and carbon emission. The results of the above cases show that the bidirectional carbon tax mechanism effectively encourages the park to purchase/sell clean power to the DN and fully taps the low-carbon synergy space between the two.

5. Conclusions

This paper investigates the carbon–energy coordination between APs and DNs based on the theory of CEF. Firstly, it improves the CEF model of the biogas CHP with carbon capture in APs, and addresses the calculation of the carbon intensity of surplus power exported from AP to DN under the carbon-emitting characteristics of greenhouse loads in APs. Based on the above model and considering the bidirectional interactions of electric power and carbon emission between the park and the distribution network, the low-carbon coordination potential between them is explored, and a Stackelberg game approach is employed to achieve integrated dynamic pricing of purchase and sale electricity prices and carbon taxes. The main conclusions are as follows:

(1) The CC-CHP carbon emission flow model proposed in this paper can account for the carbon emissions associated with energy consumption, such as the electricity used by carbon capture equipment and the heat consumed for biogas pool heating. It effectively describes the complex carbon–energy coupling relationship in CHP and accurately calculates the carbon intensity of electricity and heat at the CHP output ports.

(2) Based on the carbon intensity calculation method for surplus electricity exported from AP to DN, which considers the 'accumulation and allocation' of greenhouse load carbon emissions proposed in this paper, the carbon intensity of the electricity

returned by prosumers can be obtained while taking into account the carbon emission of end-use loads.

(3) Compared with various cases that do not consider carbon emission flow and interact with fixed carbon emission factors, the carbon–energy collaborative case for AP and DN based on bidirectional carbon emission flow proposed in this paper reduces the overall operating cost of the distribution network and has significant low-carbon benefits for both parties.

Future research can be expanded in the following directions: The 'coordinated dispatch of AP and DN' proposed in this paper is essentially a deterministic dispatch model. In the next step, uncertain factors, such as meteorological conditions (e.g., solar radiation and temperature) and the willingness of agricultural production loads to participate in demand response, can be incorporated into the dispatch model. Additionally, the location of the AP and PV and other resources is very important for the results, and as the location of the RES changes, the results should be very different. Thus, future work also can consider the low-carbon planning problem of the DN and AP based on CEF.

Author Contributions: Conceptualization, J.G.; methodology, J.G. and X.Z.; software, J.G.; validation, J.G.; formal analysis, J.G. and H.C.; investigation, H.C.; resources, J.G.; data curation, H.C.; writing—original draft preparation, J.G. and H.C.; writing—review and editing, J.G. and H.C.; visualization, X.Z.; supervision, X.Z. All authors have read and agreed to the published version of the manuscript.

Funding: This research received no external funding.

Data Availability Statement: Data in this article is at: http://doi.org/10.13140/RG.2.2.24107.76324.

Conflicts of Interest: The authors declare no conflict of interest.

References

1. Chen, B.; Sun, N.; Chen, H.; Zhang, L.; Wan, J.; Su, J. Risk Assessment Method for Power Distribution Systems Based on Spatiotemporal Characteristics of the Typhoon Disaster Chain. *Processes* **2025**, *13*, 699. [CrossRef]
2. Yao, Y.P.; Dai, J.F.; Luo, W.H.; Su, G.L. Simulation analysis of distribution of energy consumption for year round cucumber production in multi-span GH in China. *Trans. CSAE* **2011**, *27*, 273–279.
3. Niu, H.S.; Fu, X.Q. Modeling and optimization of carbon cycle of agricultural energy internet based on renewable energy. *Electr. Power Constr.* **2022**, *43*, 1–15.
4. Yin, Y.; Xi, F.M.; Bing, L.F.; Wang, J.Y.; Li, J.Y.; Du, L.Y.; Liu, L. Accounting and reduction path of carbon emission from facility agriculture in China. *Chin. J. Appl. Ecol.* **2021**, *32*, 3856–3864.
5. Zhuang, P.; Liang, H.; Pomphrey, M. Stochastic multi-timescale energy management of GH with renewable energy source. *IEEE Trans. Sustain. Energy* **2019**, *10*, 905–917. [CrossRef]
6. Fu, X.Q.; Bai, J.H.; Sun, H.B.; Zhang, Y.M. Optimizing agro-energy-environment synergy in agricultural microgrids through carbon accounting. *IEEE Trans. Smart Grid* **2024**, *15*, 4819–4834. [CrossRef]
7. Chen, Z.; Yang, J.H.; Jin, K.Y.; Hou, B.; Wang, W.Z. Control strategy of time-shift facility agriculture load and photovoltaic local consumption based on energy blockchain. *Electr. Power Autom. Equip.* **2021**, *41*, 47–55.
8. Liu, X.F.; Gao, B.T.; Li, Y. Review on application of game theory in power demand side. *Power Syst. Technol.* **2018**, *42*, 2704–2711.
9. Jia, Y.C.; Wen, P.; Yan, Y.S.; Huo, L.M. Joint operation and transaction mode of rural multi microgrid and DN. *IEEE Access* **2021**, *9*, 14409–14421. [CrossRef]
10. Wang, W.Q.; Gao, H.J.; Xu, L.; Zhang, H.; Xiong, J.Y.; Jiang, S.Y. Interactive coordination optimization of electrical DN and agricultural irrigation park based on master-slave game. *Power Syst. Technol.* **2023**, *47*, 4698–4711.
11. Zhang, T.; Yang, J.H.; Jin, K.Y.; Li, J.B.; Yang, Z.J. Low-carbon consumption method of distributed photovoltaic for DN based on Stackelberg game. *Electr. Power Autom. Equip.* **2023**, *43*, 48–54.
12. Zhou, T.R.; Kang, C.Q.; Xu, Q.Y.; Chen, Q.X. Preliminary theoretical investigation on power system CEF. *Autom. Electr. Power Syst.* **2012**, *36*, 38–43.
13. Cheng, Y.H.; Zhang, N.; Zhang, B.S.; Kang, C.Q.; Xi, W.M.; Feng, M.S. Low-carbon operation of multiple energy systems based on energy-carbon integrated prices. *IEEE Trans. Smart Grid* **2020**, *11*, 1307–1318. [CrossRef]

14. Zhang, N.; Li, Y.W.; Huang, J.H.; Li, Y.H.; Du, E.S.; Li, M.X.; Liu, Y.L.; Kang, C.Q. Carbon measurement method and carbon meter system for whole chain of power system. *Autom. Electr. Power Syst.* **2023**, *47*, 2–12.
15. Zhou, T.R.; Kang, C.Q. Research on Low-carbon Oriented Optimal Operation of DNs Based on CEF Theory. *J. Global Energy Intcon.* **2019**, *2*, 241–247.
16. Yu, C.T.; Liang, S.Q.; Zhang, L.J.; Gao, M.J.; Huang, J.Q.; Zhu, Y.H.; Liu, T.W.; Bian, X.Y. Low carbon economic optimization dispatching of medium and low voltage distribution systems based on CEF. In Proceedings of the 2023 8th International Conference on Power and Renewable Energy (ICPRE), Shanghai, China, 25 September 2023.
17. Yan, J.W.; Tan, L.; Liu, N.; Liu, L.Y. Electricity-carbon coupling trading for multi-microgrids system based on carbon flow tracing. *Power Syst. Technol.* **2023**, *48*, 39–49.
18. Wang, C.Q.; Chen, Y.; Wen, F.S.; Tao, Y.; Chi, C.Y.; Jiang, X.D. Improvement and perfection of CEF theory in power systems. *Power Syst. Technol.* **2022**, *46*, 1683–1691.
19. Fan, S.L.; Xu, G.D.; Chen, Z.P.; Xing, H.J.; Gao, Y.; Ai, Q. Carbon-embedded energy coordination strategy in park-level integrated energy system considering time-varying carbon emission measurement. *J. Cleaner Prod.* **2024**, *434*, 139967. [CrossRef]
20. Zhang, X.Y.; Wang, L.Y.; Huang, L.; Wang, S.H.; Wang, C.T.; Guo, C.X. Optimal dispatching of park-level integrated energy system considering augmented CEF and carbon trading bargain model. *Autom. Electr. Power Syst.* **2023**, *47*, 34–46.
21. Zhan, B.C.; Feng, C.S.; Wang, X.H.; Zhang, H.; Ma, J.W.; Wen, F.S. A P2P electricity-carbon trading mechanism for distributed prosumers based on CEF model. *J. Shanghai Jiaotong Univ.* **2023**, *58*, 1846–1856.
22. Liang, S.Q.; Bian, X.Y.; Liu, T.W.; Yu, C.T.; Zhao, J.; Zhou, B. Low-carbon optimal dispatching method for the medium and low voltage distribution system considering the aggregated power of station resources. *Power Syst. Technol.* **2024**, *48*, 3217–3227.
23. Wan, T.; Tao, Y.C.; Qiu, J.; Lai, S.Y. Distributed energy and carbon emission right trading in local energy systems considering the emission obligation on demand side. *IEEE Syst. J.* **2023**, *17*, 6292–6301. [CrossRef]
24. Liu, L.Y.; Jiang, K.; Liu, N.; Zhang, Y.X. Multi-agent energy-carbon sharing mechanism for parks based on Stackelberg game. *Proc. CSEE* **2024**, *44*, 2119–2130.
25. Liu, Y.X.; Yao, L.Z.; Zhao, B.; Xu, J.; Liao, S.Y.; Pang, X.P. Low-carbon economic dispatch of DN-microgrid clusters considering flexible clustering. *Autom. Electr. Power Syst.* **2024**, *48*, 59–68.
26. Tan, H.; Li, Z.X.; Wang, Q.J.; Mohamed, M.B. A novel forecast scenario-based robust energy management method for integrated rural energy systems with greenhouses. *Appl. Energy* **2023**, *330*, 120343. [CrossRef]
27. Tan, H.; Yan, W.; Wang, H. Optimal Dispatch Model of Biogas-wind-solar Isolated Multi-energy Micro-grid Based on Thermal Energy Flow Analysis of Buildings. *Power Syst. Technol.* **2020**, *44*, 2483–2491.
28. Wang, Y.Q.; Gao, S.; Jia, W.H.; Ding, T.; Zhou, Z.Y.; Wang, Z.K. Data-driven distributionally robust economic dispatch for park integrated energy systems with coordination of carbon capture and storage devices and combined heat and power plants. *IET Renew. Power Gen.* **2022**, *16*, 2617–2629. [CrossRef]
29. Farivar, M.; Low, S. Branch flow model: Relaxations and convexification—Part I. *IEEE Trans. Power Syst.* **2013**, *28*, 2554–2564. [CrossRef]
30. Zhou, T.R.; Kang, C.Q.; Xu, Q.Y.; Chen, Q.X. Preliminary investigation on a method for CEF calculation of power system. *Autom. Electr. Power Syst.* **2012**, *36*, 44–49.

Disclaimer/Publisher's Note: The statements, opinions and data contained in all publications are solely those of the individual author(s) and contributor(s) and not of MDPI and/or the editor(s). MDPI and/or the editor(s) disclaim responsibility for any injury to people or property resulting from any ideas, methods, instructions or products referred to in the content.